

N69-15714
NASA CR-99158

INVESTIGATION OF THE KINETICS OF CRYSTALLIZATION OF MOLTEN BINARY AND TERNARY OXIDE SYSTEMS

**CASE FILE
COPY**

H910373-13

by

James F. Bacon and Robert B. Graf

JANUARY 1, 1969

United Aircraft Research Laboratories



SUMMARY & QUARTERLY STATUS REPORT NO. 13

CONTRACT NASW-1301

United Aircraft Research Laboratories



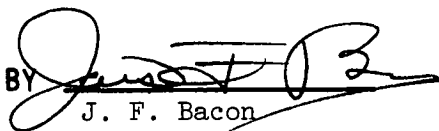
EAST HARTFORD, CONNECTICUT

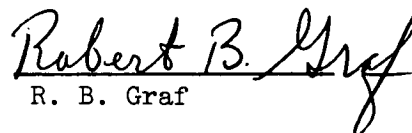
Investigation of the Kinetics of Crystallization of
Molten Binary and Ternary Oxide Systems

Summary and Quarterly Status Report No. 13

Contract NASW-1301

REPORTED BY


J. F. Bacon


R. B. Graf

APPROVED BY



M. A. DeCrescnete, Chief
High Temperature Materials

DATE 1/1/69

NO. OF PAGES 73

COPY NO.

Investigation of the Kinetics of Crystallization of

Molten Binary and Ternary Oxide Systems

Summary and Quarterly Status Report No. 13

TABLE OF CONTENTS

	<u>Page</u>
SUMMARY	1
INTRODUCTION	1
SELECTION AND PREPARATION OF GLASS SYSTEMS FOR PRELIMINARY EVALUATION	3
Low Atomic Number Oxide Components are Primary Choice	3
Moduli-Density Values for Several Low Atomic Number Oxides	3
Results with Cordierite Glasses Indicate Need for Further Work.	4
Glasses Analogous to "Invert" Glasses Show Best Results to Date	4
Compositional Changes to Improve Workability of "Invert" Glasses	15
Mathematical Analysis in Search of Optimal Compositions	18
Preliminary Exploration of Effect of Microstructure on Mechanical Properties of Two-Phase Glasses	18
Methods Used in Preparing Selected Glasses	22
DIRECT OPTICAL OBSERVATIONS OF THE KINETICS OF GLASS CRYSTALLIZATION	23
Estimation of Liquidus and Working Range	23
Role of Lanthana in Kinetics of Crystallization of UARL Cordierite Based Glasses	25
CHARACTERIZATION OF EXPERIMENTAL GLASSES BASED ON BULK SPECIMENS	28
Density Measurements	28
Young's Modulus for Glass Rods Aspirated Directly from Melt	29
FIBERIZABILITY STUDIES	38
Young's Modulus for Mechanically Drawn Experimental Glass Fibers Evaluated by Mechanical Tests	38

TABLE OF CONTENTS (Contd.)

	<u>Page</u>
Young's Modulus for Mechanically Drawn Experimental Glass Fibers Evaluated by Ultrasonic Pulse Techniques	43
Purchase of Single Hole Platinum Bushings for Improving Fiberization Processes	44
CONCLUSIONS	45
PERSONNEL ACTIVE ON PROGRAM	46
REFERENCES	47
FIGURES 1 - 24	49

LIST OF TABLES

<u>No.</u>		<u>Page</u>
I	New Experimental Glass Batches Actual Ingredients in Grams	5
II	Liquidus Temperature and Working Characteristics of Several UARL Invert Analog Glasses	26
III	Summary of All Density Determinations for Bulk Specimens of UARL Experimental Glasses	30
IV	Summary of All Values for Young's Modulus Measured on Circular Rods Formed Directly from Melt	32
V	Reproducibility of Values of Young's Modulus Measured on Rods Aspirated Directly from Melt	35
VI	Values for Young's Modulus on Mechanically Drawn Fibers of UARL Experimental Glasses as Determined by Measurements on Tensile Test Equipment	40
VII	Correlation Between Standard Deviation in Young's Modulus for Mechanically Drawn Fibers Measured on Tensile Equipment and Standard Deviation in Diameter	42

LIST OF FIGURES

<u>No.</u>	
1	Structure in Glass - 278
2	Structure in Glass - 278a
3	Structure in Glass - 278b
4	Structure in Glass - 279a
5	Structure in Glass - 279a
6	Structure in Glass - 279bi
7	Structure in Glass - 279bo
8	Structure in Glass - 280a
9	Structure in Glass - 280
10	Structure in Glass - 281
11	Structure in Glass - 281b
12	Structure in Glass - 282
13	Structure in Glass - 282
14	Structure in Glass - 282a
15	Close-up of Micro-furnace, Heat Shields Removed
16	Micro-furnace in Position for Use
17	Light Photomicrographs Showing the Approximate Locations of Beam Scan Analyses
18a	Electron Beam Scan Analysis of Area 1 as Indicated in Fig. 1B. The Crystals
18b	Electron Beam Scan Analysis of Area 2 as Indicated in Fig. 1B.
19	Schematic Representation of the Paths Scanned by the Electron Beam
20a	Lanthanum Distribution Scans Across Path Shown Schematically in Fig. 19 - Scan 1
20b	Lanthanum Distribution Scans Across Path Shown Schematically in Fig. 19 - Scan 2

LIST OF FIGURES (Cont'd)

<u>No.</u>	
20c	Lanthanum Distribution Scans Across Path Shown Schematically in Fig. 19 - Scan 3
20d	Lanthanum Distribution Scans Across Path Shown Schematically in Fig. 19 - Scan 4
20e	Lanthanum Distribution Scans Across Path Shown Schematically in Fig. 19 - Scan 5
20f	Lanthanum Distribution Scans Across Path Shown Schematically in Fig. 19 - Scan 6
21	Demonstration of Circularity of Mechanically Drawn Fibers
22	Platform Kiln Used for Fiberizability Studies
23	Platform Kiln in Use for Mechanically Drawing Glass Fibers
24	UARL Design for Single-Hole Bushing Patterned after those of Tiede (Ref. 32) and Mat. Bur. Standards (Ref. 33)

Investigation of the Kinetics of Crystallization of

Molten Binary and Ternary Oxide Systems

Summary and Quarterly Status Report No. 13 - March 1, 1968 through November 30, 1968

Contract No. NASW-1301

SUMMARY

This report deals in detail with the work carried out in the thirteenth quarter of Contract NASW-1301, a period which started September 1, 1968 and ended November 30, 1968. The report also summarizes the research of the nine-month contractual period starting March 1, 1968 and ending November 30, 1968. In the nine-month period eighty-three new glass compositions were prepared and partially characterized through various property measurements such as density, modulus and fiberizability. The research program recently has comprised essentially three areas, the cordierite-rare earth and/or zirconia glass region, the UARL invert analog glass systems, and a preliminary evaluation of the mechanical properties of two-phase glass systems.

Good results to date have been obtained in the UARL invert analog glass series where several compositions have been found with values for Young's modulus of 20.7, 20.19, 20.25 million psi for bulk samples, and for the 20.7 million psi samples a specific modulus of 6.82 million psi per gram per cubic centimeter. Equally good results are shown by the cordierite-rare earth and/or zirconia system with glasses having moduli of 22.36, 20.12, and 19.23 million psi for bulk samples and with a specific modulus again in hybrid units of 7.38 for the highest one of these. A promising new direction has been found based on the fact that in some glasses a second phase due to heat treatment develops so rapidly that it is present in glass fibers drawn at high rates of speed with a resultant improvement in modulus.

INTRODUCTION

This is the thirteenth quarterly report for Contract NASW-1301 entitled "Investigation of the Kinetics of Crystallization of Molten Binary and Ternary Oxide Systems." It is also the summary report for the fourth contractual period which included the eleventh, twelfth, and thirteenth quarters. The twelfth quarter started September 1, 1968 and ended November 30, 1968 while the nine-month contractual extension period ran from March 1, 1968 through November 30, 1968.

The primary objective of this contract is to gain a better understanding of the mechanisms of glass formation by measuring the rate at which crystallization occurs and the effect of antinucleating agents on the observed crystallization rate for systems which tend to form complex three-dimensional structures. The molten oxide systems selected for study, the reasons for their selection, and the methods used to prepare them form the first major section of this report. It will be noted that the report emphasizes those molten oxide systems that tend to form complex three-dimensional structures such as rings or interpenetrating layers since this approach, as will be shown, has resulted in several new glass compositions with increased values for Young's modulus.

The research, therefore, continues to emphasize the viewpoint that glass formation must be considered as a rate phenomenon and will continue to concentrate on systems that tend to form complex many-atom three-dimensional molecules and which have suitable viscosity and surface tension to permit mechanical drawing of glass fibers. This view of the glass formation process justifies the consideration of oxide systems previously thought impractical and allows the search for systems that may yield high-strength, high-modulus glass fibers to be carried out on an unusually broad basis.

In addition, the research indicates that the effect of microstructure of a glass on its mechanical properties should be studied since the answer to such a program is not predictable from any surmise while preliminary experiments at UARL indicate both that such structures may increase the modulus and can be induced in mechanical drawn fibers without any alteration in the drawing process.

Measurement of crystallization rates in molten oxides using microscopic observations and a microfurnace proved that lanthanum oxide successfully lowered the rate of crystallization for glasses in the cordierite field. In this quarter the electron microprobe was used to investigate the role played by lanthanum oxide in crystallization kinetics and the results are reported in the second section of the report. Observations of the liquidus and working range using the same equipment proved very helpful in deciding which compositions could be successfully fiberized and these observations are also included in this second report section.

Characterization of the experimental glasses produced as bulk specimens is the subject of the third section of the report. Such characterization is largely achieved by measuring the density, and determining Young's modulus for bulk samples of the experimental glasses. Originally, specimens for measuring Young's modulus of bulk glasses were made by first casting a glass slab, annealing it, and then cutting rectangular bars from the slab by precision optical grinding techniques. Now, however, we form samples suitable for modulus determinations by pulling molten glass into fused silica tubes by the use of controlled suction with hypodermic syringes so that such measurement of Young's modulus is now much cheaper and more expedient.

The actual making of a glass fiber from a given composition is, of course, the best test for the fiberizing characteristics of that composition and details of this process together with the evaluation of Young's modulus for the glass fiber form the fourth and concluding section of the experimental data.

SELECTION AND PREPARATION OF GLASS SYSTEMS FOR PRELIMINARY EVALUATION

Low Atomic Number Oxide Components are Primary Choice

Since the ultimate long-range objective of this program is the attainment of high-modulus, high-strength-to-density continuous vitreous fibers, research will be largely concentrated on complex molecules composed of low atomic number oxides such as those shown in the tabulation below (Ref. 1).

Moduli-Density Values for Several Low Atomic Number Oxides

Oxide	Young's	Density (gms/cm ³)	Maximum Strength (5% Strain - 10 ⁶ psi)	Modulus
	Modulus (10 ⁶ psi)			Density Ratio 10 ⁶ psi/gms/cm ³
Al ₂ O ₃	76	4.0	3.8	19
BeO	51	3.0	2.6	17
MgO	35	3.5	1.8	10
SiO ₂	10.5	2.2	0.53	5
MgO Al ₂ O ₃	35	3.6	1.8	10
TiO ₂	41	4.26	2.06	9.6

For this reason, specific molecular systems considered have been silicates (since silica is the best-known glass former) such as cordierite, Al₃Mg₂(Si₅Al)O₁₈, known to have a ring crystal structure with ions arranged in sheets but not a layer structure (Ref. 2); benitoite, BaTiSi₃O₉, likewise a complex three-dimensional structure (Ref. 2); and beryl, Be₃Al₂Si₆O₁₈, a ring structure like that of cordierite. The low value for silica in contrast to the other oxides indicate that the percentage of silica in such a glass must be held at a minimum if high moduli are to be achieved. The major constituent, silica which provides the glass structure and the desired viscosity characteristics, can be regarded as a necessary evil and the positive direction for modulus improvement clearly lies in using no more silica than necessary and so leads to the consideration of invert analog glasses as we show in a later section. It is only natural, also that one should devote some attention to glass systems other than silica and UARL continues its efforts in this area although all such nonsilica systems prepared by us to date have such high densities that specific moduli are very disappointing as shown in our earlier reports.

Results with Cordierite Glasses Indicate Need for Further Work

Eighty-three new glass compositions were conceived, prepared, melted and partially characterized in this nine-month period increasing the number of original glass formulations studied under this program to three hundred and forty-nine. Compositions for all new glasses prepared are shown in Table I. Glasses 262 and 263 of Table Ia, 304, 305 and 306 of Table Ie and 319, 320 and 321 of Table If below belong to the cordierite glass system with extensive additions of rare earths as major constituents. Cordierite or $\text{Mg}_2\text{Al}_4\text{Si}_5\text{O}_{18}$ is a three-dimensional ring former, as discussed in earlier UARL reports (UARL E910373-4 et seq.), and these glasses that include major quantities of one of the rare earths such as lanthana, ceria or yttria are delayed in devitrification by the additions (UARL G910373-11 and this report). Zirconia has been found to show a similar effect on the devitrification rate for cordierite glasses. The rare earth additions and the zirconia addition also markedly increase the elastic modulus of the glasses of the cordierite family. As will be apparent later in this report (Table IV) elastic moduli as high as 19.23 million psi are obtainable for bulk specimens of the cordierite glass system without any toxic components such as beryllia.

Glasses Analogous to "Invert" Glasses Show Best Results to Date

The very new UARL experimental glasses considered in this section of the report belong to a region of glass composition analogous to Stevels' "invert" glasses.

The concept developed by J. M. Stevels and his associates from 1954 on was that by a proper combination of oxides, stable metasilicate glasses could be obtained. A typical example cited by Stevels is 50 mol % SiO_2 and 12.5 mol % of the four materials Na_2O , K_2O , CaO , BaO . Dr. Stevels explained this "anomalous" case of glass formation by saying that "by choosing a batch with a great number of network modifiers the 'glue' between the chains is so irregular that crystallization is prevented." Obviously, by using a combination of alkali oxides and a combination of alkaline earth oxides as preferred by Stevels, the liquidus temperature can be lowered and the field of glass formation can be increased.

Weyl (Ref. 3) states further that Trap and Stevels characterized the coherence of their silicate glasses by a structural parameter Y denoting the average number of bridging ions per SiO_4^{4-} tetrahedron. This parameter may be calculated from the expression

$$Y = 6 - \frac{200}{P} \quad \text{where } P = \text{mol \% SiO}_2$$

so that when $P = 33\frac{1}{3}$, $Y = 0$ and SiO_4^{4-} groups are isolated; when $P = 40\%$, $Y = 1$ and on the average SiO_4^{4-} groups appear in pairs. Commercial silicate glasses, on the other hand, have Y values between 3.0 and 3.5 in agreement with the Zachareisen rules for stable glass formation which state that a stable

TABLE Ia

New Experimental Glass Batches
Actual Ingredients in Grams

<u>Actual Ingredient</u>	<u>262</u>	<u>263</u>	<u>264</u>	<u>265</u>
Boric Acid (fused)	---	---	29.4	---
Barium Carbonate	---	---	153.2	---
Titanium Dioxide	---	---	359.0	---
Sodium Carbonate	---	---	9.4	---
Silica	345.5	175.5	---	128.5
Alumina	105.0	56.5	---	65.4
Magnesia	13.5	7.35	---	25.9
Beryllium Carbonate	75.6	---	---	---
Lanthanum Oxalate	---	542.0	---	442.0
Zinc Carbonate	---	---	---	80.3
Lithium Carbonate	---	---	---	47.4

TABLE Ib

New Experimental Glass Batches
Actual Ingredients in Grams

<u>Actual Ingredient</u>	<u>266</u>	<u>267</u>	<u>268</u>	<u>269</u>	<u>270</u>	<u>271</u>
Silica	122.3	168.8	114.8	76.3	107.0	97.4
Alumina	124.3	133.5	109.3	90.5	58.1	52.9
Lithium Carbonate	90.6	98.0	79.2	65.8	79.2	72.2
Calcium Carbonate	122.5	131.2	107.2	88.9	106.8	97.3
Magnesia	49.4	52.8	43.0	35.8	43.1	39.2
Yttrium Oxalate	---	---	---	---	301.0	---
Lanthanum Oxalate	---	---	---	---	---	319.5
Beryllium Carbonate	---	69.0	---	---	---	---
Zinc Carbonate	154.0	---	143.6	118.8	134.3	122.2
Zirconium Carbonate	---	---	53.0	44.0	---	---
Cerium Oxalate	---	---	---	224.3	---	---
	<u>272</u>	<u>273</u>	<u>274</u>	<u>275</u>	<u>276</u>	<u>277</u>
Silica	85.8	177.0	132.3	183.0	202.0	129.7
Alumina	---	120.4	134.7	51.6	57.2	44.0
Lithium Carbonate	63.5	87.2	97.3	---	46.6	33.1
Calcium Carbonate	85.5	118.0	---	---	---	---
Magnesia	34.6	47.6	53.4	---	---	---
Yttrium Oxalate	---	---	---	---	---	---
Lanthanum Oxalate	615.0	---	---	358.0	395.0	303.0
Beryllium Carbonate	44.9	113.2	69.5	78.8	87.5	67.0
Zinc Carbonate	---	---	158.0	70.2	---	---
Zirconium Carbonate	---	---	---	---	---	---
Cerium Oxalate	---	---	---	---	---	305.0

TABLE Ic

New Experimental Glass Batches
Actual Ingredients in Grams

<u>Actual Ingredient</u>	<u>278</u>	<u>279</u>	<u>280</u>	<u>281</u>	<u>282</u>
SiO ₂	325	325	333.3	275	150
Boric Acid Fused	---	---	243	222	444
Barium Carbonate	---	---	---	128.5	128.5
TiO ₂ (not rutile)	100	---	---	---	---
Zirconium Carbonate	---	112.4	---	---	---
Calcium Carbonate	44.6	---	---	---	---
Zinc Carbonate	---	38.6	---	---	---
Lithium Carbonate	123.5	61.8	---	---	---
Sodium Carbonate	---	42.8	48.6	---	---

TABLE Id

New Experimental Glass Batches
Actual Ingredients in Grams

<u>Actual Ingredient</u>	<u>283</u>	<u>284</u>	<u>285</u>	<u>286</u>	<u>287</u>	<u>288</u>	<u>289</u>
Silica	92.4	92.4	79.9	96.5	63.4	80.2	79.5
Aluminum Oxide	50.2	50.2	65.1	65.5	64.4	65.4	64.8
Lithium Carbonate	68.2	68.2	47.2	45.6	46.7	47.4	46.9
Calcium Carbonate	12.3	12.3	---	---	---	---	---
Zinc Carbonate	116.0	61.7	80.0	80.6	78.9	40.3	79.5
Magnesium Oxide	37.2	37.3	25.8	25.9	25.5	25.9	25.6
Boric Acid Fused	80.0	79.7	99.0	66.1	130.2	98.8	58.9
Lanthanum Oxalate	309.5	303.5	442.0	439.0	436.0	440.0	435.0
Cerium Oxalate	21.9	21.7	---	---	---	---	---
Zirconium Carbonate	17.7	17.8	---	---	---	---	---
Cupric Carbonate	---	55.2	---	---	---	41.1	40.6
	<u>290</u>	<u>291</u>	<u>292</u>	<u>293</u>	<u>294</u>	<u>295</u>	<u>296</u>
Silica	104.2	90.5	79.9	104.7	63.4	83.6	84.4
Aluminum Oxide	56.6	73.9	65.2	56.8	57.4	56.7	57.2
Lithium Carbonate	74.2	53.5	47.2	61.9	78.2	77.2	77.6
Calcium Carbonate	---	---	---	104.3	105.4	34.7	70.5
Zinc Carbonate	126.0	90.6	79.9	104.7	132.4	130.8	132.0
Magnesium Oxide	42.0	29.2	25.8	33.7	42.6	42.1	42.4
Boric Acid Fused	128.9	112.0	98.5	77.5	86.9	128.9	86.7
Lanthanum Oxalate	293.0	---	439.0	---	---	---	---
Yttrium Oxalate	---	438.0	---	294.5	297.4	295.0	297.0
	<u>297</u>	<u>298</u>	<u>299</u>	<u>300</u>	<u>301</u>	<u>302</u>	<u>303</u>
Silica	107.3	97.5	99.8	132.7	97.3	102.2	104.8
Aluminum Oxide	58.2	52.9	54.1	---	52.8	55.4	56.8
Lithium Carbonate	79.1	72.1	73.4	97.1	71.8	40.3	77.2
Calcium Carbonate	107.2	97.5	99.7	132.5	97.3	102.2	55.8
Zinc Carbonate	71.5	65.2	---	166.3	121.8	127.8	131.0
Magnesium Oxide	43.2	39.3	40.2	53.4	39.2	41.1	42.2
Boric Acid Fused	---	---	122.8	163.8	---	---	---
Lanthanum Oxalate	---	320.0	328.0	---	---	---	---
Yttrium Oxalate	305.0	---	---	---	---	288.0	295.0
Cupric Oxide	39.7	36.2	---	---	---	38.9	38.8
Rare Earth Oxalate	---	---	---	---	322.0	---	---

Table Ie

New Experimental Glass Batches
Actual Ingredients in Grams

<u>Actual Ingredient</u>	<u>283</u>	<u>284</u>	<u>285</u>	<u>286</u>	<u>287</u>	<u>288</u>
Silica	92.4	92.4	79.9	96.5	63.4	80.2
Aluminum Oxide	50.2	50.2	65.1	65.5	64.4	65.4
Lithium Carbonate	68.2	68.2	47.2	45.6	46.7	47.4
Calcium Carbonate	12.3	12.3	----	----	----	----
Zinc Carbonate	116.0	61.7	80.0	80.6	78.9	40.3
Magnesium Oxide	37.2	37.3	25.8	25.9	25.5	25.9
Boric Acid (fused)	80.0	79.7	99.0	66.1	130.2	98.8
Lanthanum Oxalate	309.5	303.5	442.0	439.0	436.0	440.0
Cerium Oxalate	21.9	21.7	-----	-----	-----	-----
Zirconium Carbonate (nominal)	17.7	17.8	-----	-----	-----	-----
Titanium Dioxide	----	----	-----	-----	-----	----
Cupric Carbonate	----	55.2	-----	-----	-----	41.1
Yttrium Oxalate	----	----	-----	-----	-----	----
Cupric Oxide	----	----	-----	-----	-----	----
Rare Earth Oxalate	----	----	-----	-----	-----	----
Cobaltous Carbonate	----	----	-----	-----	-----	----
	<u>289</u>	<u>290</u>	<u>291</u>	<u>292</u>	<u>293</u>	<u>294</u>
Silica	79.5	104.2	90.5	79.9	104.7	63.4
Aluminum Oxide	64.8	56.6	73.9	65.2	56.8	57.4
Lithium Carbonate	46.9	74.2	53.5	47.2	61.9	78.2
Calcium Carbonate	----	----	----	----	104.3	105.4
Zinc Carbonate	79.5	126.0	90.6	79.9	104.7	132.4
Magnesium Oxide	25.6	42.0	29.2	25.8	33.7	42.6
Boric Acid (fused)	58.9	128.9	112.0	98.5	77.5	86.9
Lanthanum Oxalate	435.0	293.0	----	439.0	----	----
Cerium Oxalate	----	----	----	----	----	----
Zirconium Carbonate (nominal)	----	----	----	----	----	----
Titanium Dioxide	----	----	----	----	----	----
Cupric Carbonate	40.6	----	----	----	----	----
Yttrium Oxalate	----	----	438.0	----	294.5	297.4
Cupric Oxide	----	----	----	----	----	----
Rare Earth Oxalate	----	----	----	----	----	----
Cobaltous Carbonate	----	----	----	----	----	----

Table Ie (con'td)

New Experimental Glass Batches
Actual Ingredients in Grams

<u>Actual Ingredient</u>	<u>295</u>	<u>296</u>	<u>297</u>	<u>298</u>	<u>299</u>	<u>300</u>	<u>301</u>
Silica	83.6	84.4	107.3	97.5	99.8	132.7	97.3
Aluminum Oxide	56.7	57.2	58.2	52.9	54.1	----	52.8
Lithium Carbonate	77.2	77.6	79.1	72.1	73.4	97.1	71.8
Calcium Carbonate	34.7	70.5	107.2	97.5	99.7	132.5	97.3
Zinc Carbonate	130.8	132.0	71.5	65.2	----	166.3	121.8
Magnesium Oxide	42.1	42.4	43.2	39.3	40.2	53.4	39.2
Boric Acid (fused)	128.9	86.7	----	----	122.8	163.8	----
Lanthanum Oxalate	----	----	----	320.0	328.0	----	----
Cerium Oxalate	----	----	----	----	----	----	----
Zirconium Carbonate (nominal)	----	----	----	----	----	----	----
Titanium Dioxide	----	----	----	----	----	----	----
Cupric Carbonate	----	----	----	----	----	----	----
Yttrium Oxalate	295.0	297.0	305.0	----	----	----	----
Cupric Oxide	----	----	39.7	36.2	----	----	----
Rare Earth Oxalate	----	----	----	----	----	----	322.0
Cobaltous Carbonate	----	----	----	----	----	----	----
	<u>302</u>	<u>303</u>	<u>304</u>	<u>305</u>	<u>306</u>	<u>307</u>	<u>308</u>
Silica	102.2	104.8	133.0	133.0	134.0	106.0	107.7
Aluminum Oxide	55.4	56.8	96.6	96.7	97.0	57.6	58.4
Lithium Carbonate	40.3	77.2	----	----	----	67.6	79.5
Calcium Carbonate	102.2	55.8	----	----	----	105.8	107.2
Zinc Carbonate	127.8	131.0	79.2	76.5	40.0	70.7	54.0
Magnesium Oxide	41.1	42.2	76.4	----	77.0	42.7	43.4
Boric Acid (fused)	----	----	----	----	----	----	----
Lanthanum Oxalate	----	----	----	----	----	----	----
Cerium Oxalate	----	----	----	----	----	----	----
Zirconium Carbonate (nominal)	----	----	----	----	----	----	----
Titanium Dioxide	----	----	----	----	----	----	----
Cupric Carbonate	----	----	----	----	----	----	----
Yttrium Oxalate	288.0	295.0	381.0	384.4	384.0	299.0	303.0
Cupric Oxide	38.9	38.8	----	25.2	----	39.4	28.6
Rare Earth Oxalate	----	----	----	----	----	----	----
Cobaltous Carbonate	----	----	----	----	51.0	22.7	46.1

TABLE If

New Experimental Glass Batches
Actual Ingredients in Grams

<u>Actual Ingredient</u>	<u>309</u>	<u>310</u>	<u>311</u>	<u>312</u>	<u>313</u>
Silica	170.9	146.7	124.1	102.8	82.1
Aluminum Oxide	64.5	74.6	84.2	93.1	100.2
Lithium Carbonate	46.7	54.2	60.9	67.2	72.4
Calcium Carbonate	-----	-----	-----	-----	-----
Zinc Carbonate	-----	-----	-----	-----	-----
Magnesium Oxide	-----	-----	-----	-----	-----
Beryllium Carbonate	83.1	80.4	77.4	74.7	71.7
Yttrium Oxalate	-----	-----	-----	-----	-----
Lanthanum Oxalate	446	473	499	522	551
Cerium Oxalate	-----	-----	-----	-----	-----
Zirconium Carbonate (nom.)	-----	-----	-----	-----	-----
Cupric Oxide	-----	-----	-----	-----	-----
	<u>314</u>	<u>315</u>	<u>316</u>	<u>317</u>	<u>318</u>
Silica	140.0	147.0	141.9	142.6	238
Aluminum Oxide	71.3	62.3	60.2	60.5	134.6
Lithium Carbonate	52.0	45.2	43.7	43.9	-----
Calcium Carbonate	-----	61.2	-----	-----	-----
Zinc Carbonate	-----	-----	74.0	-----	-----
Magnesium Oxide	58.7	24.7	23.8	23.9	106.4
Beryllium Carbonate	-----	32.2	31.0	31.2	46.2
Yttrium Oxalate	-----	-----	-----	-----	-----
Lanthanum Oxalate	453	430	415	418	-----
Cerium Oxalate	-----	-----	-----	-----	-----
Zirconium Carbonate (nom.)	-----	-----	-----	-----	-----
Cupric Oxide	-----	-----	-----	47.2	-----

TABLE If (Contd.)

New Experimental Glass Batches
Actual Ingredients in Grams

<u>Actual Ingredient</u>	<u>319</u>	<u>320</u>	<u>321</u>	<u>322</u>	<u>323</u>	
Silica	155.5	202.6	141.0	178.0	195.4	
Aluminum Oxide	88.0	114.7	89.6	129.7	142.0	
Lithium Carbonate	----	----	----	----	68.6	
Calcium Carbonate	----	----	----	----	----	
Zinc Carbonate	----	----	----	106.0	----	
Mangesium Oxide	69.5	90.6	70.9	102.4	112.3	
Beryllium Carbonate	----	----	----	45.3	48.7	
Yttrium Oxalate	----	----	531	----	----	
Lanthanum Oxalate	404	----	----	----	----	
Cerium Oxalate	----	----	----	----	----	
Zirconium Carbonate (nom.)	----	104	----	----	----	
Cupric Oxide	----	----	----	----	----	
	<u>324</u>	<u>325</u>	<u>326</u>	<u>327</u>	<u>328</u>	<u>329</u>
Silica	161.9	124.4	144.8	189.7	88.0	76.4
Aluminum Oxide	109.7	70.3	81.9	62.0	49.7	64.8
Lithium Carbonate	79.3	51.2	59.6	45.0	36.1	47.0
Calcium Carbonate	----	----	----	----	----	----
Zinc Carbonate	134.7	86.6	100.7	76.4	61.2	79.5
Magnesium Oxide	86.8	55.6	64.7	48.9	39.4	51.1
Beryllium Carbonate	47.1	36.2	42.2	----	----	----
Yttrium Oxalate	----	417	----	368	294	384
Lanthanum Oxalate	----	----	----	----	344	----
Cerium Oxalate	----	----	----	----	----	----
Zirconium Carbonate (nom.)	----	----	111.4	84.4	----	88.2
Cupric Oxide	----	----	----	----	----	----

Table Ig

New Experimental Glass Batches
Actual Ingredients in Grams

<u>Actual Ingredient</u>	<u>330</u>	<u>331</u>	<u>332</u>	<u>333</u>	<u>334</u>
Silica	129.2	148.8	123.8	142.1	117.9
Aluminum Oxide (c.p.)	67.4	77.5	64.7	74.0	85.8
Magnesium Oxide (c.p.)	----	----	53.4	60.9	67.8
Yttrium Oxalate	----	460	----	439	----
Lanthanum Oxalate	466	----	447	----	395
Zirconium Carbonate (nom.)	----	----	----	----	----
Beryllium Carbonate	98.3	113	----	----	----
Zinc Carbonate (c.p.)	82.9	95.4	79.6	91.0	70.2
Lithium Carbonate (c.p.)	----	----	----	----	----
Calcium Carbonate (c.p.)	----	----	----	----	----
Cupric Oxide	----	----	----	----	----
Cobaltous Carbonate (c.p.)	----	----	----	----	----
Cerium Oxalate	----	----	----	----	----
Boric Acid Fused	----	----	----	----	----
	<u>335</u>	<u>336</u>	<u>337</u>	<u>338</u>	<u>339</u>
Silica	124.3	140.7	107.6	93.8	98.5
Aluminum Oxide (c.p.)	90.4	102.5	91.2	79.3	83.5
Magnesium Oxide (c.p.)	----	----	72.1	62.8	----
Yttrium Oxalate	----	405	450	----	----
Lanthanum Oxalate	416	----	----	459	480
Zirconium Carbonate (nom.)	----	----	----	----	----
Beryllium Carbonate	121.8	143.1	----	----	116.9
Zinc Carbonate (c.p.)	74.2	84.2	93.3	81.3	85.5
Lithium Carbonate (c.p.)	----	----	----	----	----
Calcium Carbonate (c.p.)	----	----	----	----	----
Cupric Oxide	----	----	----	----	----
Cobaltous Carbonate (c.p.)	----	----	----	----	----
Cerium Oxalate	----	----	----	----	----
Boric Acid Fused	----	----	----	----	----

Table Ig (Contd.)

New Experimental Glass Batches
Actual Ingredients in Grams

<u>Actual Ingredient</u>	<u>340</u>	<u>341</u>	<u>342</u>	<u>343</u>	<u>344</u>
Silica	106.2	109.5	127.4	111.6	181.0
Aluminum Oxide (c.p.)	72.2	61.9	71.9	63.1	102.3
Magnesium Oxide (c.p.)	56.8	48.9	28.4	24.9	40.5
Yttrium Oxalate	421	----	427	----	405
Lanthanum Oxalate	----	428	----	435	----
Zirconium Carbonate (nom.)	----	----	----	----	----
Beryllium Carbonate	75.3	42.7	100.7	88.1	71.8
Zinc Carbonate (c.p.)	88.4	75.9	88.2	77.5	----
Lithium Carbonate (c.p.)	52.2	45.0	52.1	45.6	----
Calcium Carbonate (c.p.)	----	----	----	----	----
Cupric Oxide	----	----	----	----	----
Cobaltous Carbonate (c.p.)	----	----	----	----	----
Cerium Oxalate	----	----	----	----	----
Boric Acid Fused	----	----	----	----	----
	<u>345</u>	<u>346</u>	<u>347</u>	<u>348</u>	<u>349</u>
Silica	156.9	78.0	190.9	182.9	190.9
Aluminum Oxide (c.p.)	105.9	66.0	53.9	51.8	53.9
Magnesium Oxide (c.p.)	----	26.1	----	----	----
Yttrium Oxalate	418	391	----	----	----
Lanthanum Oxalate	----	----	371	357	----
Zirconium Carbonate (nom.)	----	89.8	----	70.0	----
Beryllium Carbonate	148.0	92.2	113.3	108.3	113.3
Zinc Carbonate (c.p.)	----	81.1	66.5	----	66.5
Lithium Carbonate (c.p.)	----	47.9	----	----	----
Calcium Carbonate (c.p.)	----	----	----	----	----
Cupric Oxide	----	----	----	----	----
Cobaltous Carbonate (c.p.)	----	----	----	----	----
Cerium Oxalate	----	----	----	----	371
Boric Acid Fused	----	----	----	----	----

silicate glass should consist of SiO_4^{4-} tetrahedra sharing at least three of their corners with other SiO_4^{4-} tetrahedra. On the other hand, the "invert" glasses developed by Trap and Stevels have Y values lower than 2.0 in direct contradiction of the accepted rules for stable glass formation.

When the glass composition was changed to lower and lower SiO_2 concentrations, Trap and Stevels (Ref. 3) found that some properties such as thermal expansivity, electrical deformation losses, and viscosity go through maxima or minima reaching extreme values as the parameter Y passes through the value 2.0. It is the feeling at this laboratory, UARL, that the modulus of elasticity may likewise achieve a decided maximum. However, extensive research with the "invert" glasses in the first eight quarters of this contract failed to yield any marked change in modulus. The ninth and tenth quarters, however, yielded a sixty percent increase in modulus while research in the eleventh quarter resulted in an invert glass with an elastic modulus in excess of twenty million psi as will be shown in a later section.

Stevels' "invert" glasses comprised silica, two or more monovalent oxides, usually Na_2O and K_2O and two or more alkaline earth oxides. The UARL glasses, on the other hand, although analogous to Stevels' invert glasses, consist of silica, lithia, two or more divalent oxides or fluorides, one or more trivalent oxides, and may include a second tetravalent oxide or a pentavalent oxide. This combination of divalent and trivalent oxides has proven equally effective in blocking crystallization while yielding higher moduli. The glasses of Table I, compositions 266 through 277, 283 through 302, 309 through 318, 322 through 343, and 346 through 349 may be considered typical UARL invert analog glasses. A brief glance at the subsequent Table IV shows that with these glass compositions values like a 20.19 million psi Young's modulus with a specific modulus of 5.68 for glass 325, and 20.7 million psi for Young's modulus with a specific modulus of 6.82 may be achieved for bulk specimens indicating the need for further intensive research in this area.

Compositional Changes to Improve Workability of "Invert" Glasses

The invert glasses of Table I, while yielding high moduli, proved difficult to fiberize. The available glass literature was scrutinized in an attempt to find those additions most likely to lower the liquidus, increasing the working range, and yield viscosity temperature relationships suitable for fiberization. Examination of books and patents by Weyl and Marboe (Ref. 3), Rawson (Ref. 4), Stanworth (Ref. 5), Tiede et al (Ref. 6), Armistead (Ref. 7), Bastian (Ref. 8), and Labino (Ref. 9) yielded the following suggestions for additives to improve the fiberizability of the UARL "invert" analogues.

1. B_2O_3 - Add B_2O_3 , possibly as much as the amount of silica present but keep total of two at 40 mol % or less but probably more than 25 mol %. Effect on modulus in invert glasses is not easy to predict. At best, it will contribute slightly more than SiO_2 but at worst since it is known that in silica base glasses, the B_2O_3 contribution depends on $(R_2O-Al_2O_3)/B_2O_3$, it may contribute nothing.

B_2O_3 in silica base glasses decreases the liquidus and viscosity to a marked degree. In "inverts" it should still lower liquidus but should raise viscosity especially when substituted for CaO or MgO or ZnO.

B_2O_3 content should be greater than 8 weight % to increase stability of glass and decrease devitrification tendencies but below 13 weight % to preserve chemical durability.

B_2O_3 should markedly decrease density thus increasing specific modulus.

2. Bivalent Oxides MgO, ZnO, CaO, BeO, CuO

MgO - Add MgO since it increases modulus and the greater the percentage of MgO the longer the working range of the composition and the lower the melting temperature and softening point of the fiber (8 to 15 weight % MgO).

ZnO - Behaves like MgO as judged by refractive index, resistivity, fluorescence intensity, spectral band intensity. Does not enter holes like CaO but MgO and ZnO both enter network instead.

Use at least 2 to 8 weight % bivalent oxides such as ZnO, CdO to reduce tendency of glass to devitrify.

ZnO will improve durability but will generally increase liquidus.

Do not use MgO in amount greater than 30% by weight to avoid devitrification and, for same reason, ZnO must be less than 60% by weight.

CaO - CaO and MgO are added to keep viscosity at a minimum and normally cannot be tolerated in low liquidus glasses. Do not let sum of CaO, BeO, and MgO exceed 55 weight %. CaO must be in range of 16 to 25% by weight to prevent devitrification but the lower the silica content, the lower this range. CaO enters holes and increases density.

BeO - Use BeO in range of 10 to 12% by weight to increase modulus without attendant devitrification problems.

CuO - Add CuO in amount of 9 to 10.5 weight % while maintaining the ratio of the sum of MgO and CaO to $CuO + Al_2O_3 + Fe_2O_3 + TiO_2$ at approximately 1 to 1 to secure low softening and yield a process capable of forming ultrafine

fibers in range of 10 to 20 millionths of an inch. It is expected to yield molten glass having very high interfacial tension (viscosity) and low surface tension and softening point.

3. Al_2O_3 - Use Al_2O_3 to reduce tendency of glass to devitrify. Use Al_2O_3 in place of SiO_2 to increase modulus.

4. Other Trivalent Oxides - Fe_2O_3 , Mn_2O_3 . Up to 3 weight % Fe_2O_3 is deemed beneficial to formation of continuous fibers but no one can state why. Use 3 to 10 weight % to reduce tendency of glass to devitrify.

5. Rare Earth Trivalent Oxides such as La_2O_3 and Y_2O_3 - Our own prior experience indicates that these ingredients markedly increase the modulus but that additions must be held to reasonable amounts so that the density of the glass does not become too high. Lanthana adds to glass forming characteristics markedly. Yttria is too costly to allow large additions if the glass is to be competitive commercially.

6. Co_2O_3 - Add small amounts of cobalt oxide to reduce devitrification and to improve drawing properties. Preferred range of use seems to be 2 to 7% by weight.

7. SiO_2 - If anything, increase the SiO_2 slightly to increase viscosity (hold in range 25 to 40 weight %).

8. Other Tetravalent Oxides

CeO_2 - Add to each of the compositions to increase modulus, lower liquidus, promote continuous formation of fibers. But do not add really large amounts since it markedly increases density. Fe_2O_3 is not the full equivalent of ceria since it does not have identical effects on the liquidus.

ZrO_2 - Add to increase modulus, improve durability, decrease rate of crystal formation, increase resistance to devitrification. Up to 11 weight % ZrO_2 may be used. ZrO_2 will raise acceptable working temperature. Presumably the ZrO_2 may be partially substituted for Al_2O_3 .

TiO_2 - Add to allegedly enhance fiber formation but do not let ZrO_2 + TiO_2 exceed 25% by weight and ZrO_2 and TiO_2 must each alone be below 16 weight %.

TiO_2 and ZrO_2 improve durability, liquidus, viscosity and decrease rate of crystal formation.

9. R_2O 's - Use Li_2O only. Possesses a much higher molal modulus contribution. Use in presence of BeO to increase modulus.

The first few altered UARL invert analog glass compositions prepared in accordance with these suggestions are those of Table Id, glass compositions 283 through 303, Table If compositions 309 through 318 and 322 through 329, and Table Ig 330 through 349. As will be seen from the subsequent Table IV, the results of these preparations have not yet been fully evaluated but it is already apparent that these rules based on experiences with glasses built on silica networks may not hold for the non-network "invert" glasses. In particular, substitution of B_2O_3 for SiO_2 failed to decrease the density while the substitution of CuO for ZnO markedly lowers the density. In this respect the behavior of the CuO leads to further evidence that the CuO may actually enter the silica network as suggested by Ram et al (Ref. 10) based on viscosity measurements of copper ruby glasses. This suggestion that the CuO may be present in the actual silica network in the form of $\equiv Si-O-Cu$ just as water in glass is now believed to be present as $\equiv Si-O-H$ thus forming smaller flow units than the bigger parent unit $\equiv Si-O-Si \equiv$ so that the viscosity of glasses containing $\equiv Si-O-H$ or $\equiv Si-O-Cu$ units should be lower than that of the respective parent glasses.

Mathematical Analysis in Search of Optimal Compositions

Arrangements have been made with the UARL central computation laboratory for an examination of the results obtained for each glass composition prepared to date for which we also have modulus, density and liquidus data to see what trends may be evident. This type of analysis should be especially valuable with the invert analog glasses which in general have six to eight or more components. Data of the type that will be used in these computations is shown in Tables I through VI.

Preliminary Exploration of Effect of Microstructure on Mechanical Properties of Two-Phase Glasses

Up to the year 1952 it was customary to think of glass as a homogeneous material but the application of electron microscopy to glass research has greatly altered our concept concerning the homogeneity of glass (Refs. 10 through 29). For example, in opalescence due to the formation of small drop-shaped regions of a separation of this type has two aspects, namely, the equilibrium or decreasing compatibility of a substance and the rate of nucleation. According to Weyl (Ref. 3), the higher the temperature of a molten glass, the greater is its solvent power for noble metals such as Ag and Au , for sulfides and selenides like CdS and $CdSe$, and for oxides containing either cations with a higher charge than silicon (P^{5+} , W^{6+}) or cations too large to fit into the tetrahedral structure of the glass (Sn^{4+} , Ti^{4+}). The quantity of a compound that becomes compatible in the melting range of silicate glasses varies widely. It amounts to only a fraction of one percent for gold and copper; it is of the order of one to five percent for sulfides, selenides, phosphates and titanates, and yet in some alkali-boric oxide-silica glasses the incompatibility utilized for making a Vycor glass

amounts to nearly half the volume of the total glass. These glasses, with phase-separated droplets large enough to cause noticeable light scattering, are similar to colloidal solutions whose particles are detected and characterized by Faraday-Tyndall effect or light-scattering measurements.

A second group of glasses appear completely clear to the naked eye but, when examined by the electron microscope, they may be seen to have micelles or heterogeneities of the order of 200 to 600 Angstroms. In this respect, Weyl (Ref. 3) states that there is a strong resemblance between this description of the structure of a glass developing shrinkage voids on cooling and a liquid structure changing in the direction toward a Frenkel-type liquid on heating. Both structures are characterized by fissures and by clusters or subcolloidal micelles. The permanency of the shrinkage voids cause the glass structure to approach that of a molecular liquid and one might compare the subcolloidal micelles and the walls of the matrix with molecules having strong intramolecular and weak intermolecular forces. Weyl (Ref. 3) feels that this picture explains why a fiber of a glass with a multitude of subcolloidal micelles such as the ternary eutectic in the system $\text{Li}_2\text{O}-\text{BaO}-\text{SiO}_2$ exhibits a flexibility or ductility resembling a molecular organic polymer. Vitreous silica with a much smaller number of flaws exhibits no ductility. This concept is also associated with the sonic spectra of glasses where goblets of vitreous silica cannot be made to give a pleasant ringing sound but goblets of glasses incorporating large amounts of lead oxide do and the electron microscope readily reveals the two-phase nature of the lead silicate glasses.

Glasses also exist which are completely transparent in the quenched state but which readily develop crystal nuclei under suitable heat treatment. Such glasses have been termed neo-ceramic by Janakiramarao (Ref. 29). The resulting opaque or translucent "neo-ceramic" product acquires properties different from those of the parent glass, but still retains some of the properties of its vitreous state such as conchoidal fracture and freedom from porosity. The fact that a "neo-ceramic" glass in its quenched state is thoroughly transparent and homogeneous even when examined under an ultramicroscope and displays no Tyndall effect but develops myriads of uniformly distributed nuclei of considerable size when heat treated, indicates that crystallites existed in the parent glass. On heat treatment, the incompatibility of the structural groups and the relative freedom of ions favor the growth of the crystallites or heterogeneous regions to form nuclei or micelles of definite chemical composition at the expense of the surrounding parent glass. The nucleation and growth of finely dispersed crystals from the glass matrix, particularly if these crystals are not cubic but have one dimension appreciably larger than other dimensions, allows the possibility of noteworthy amounts of crystal orientation or whisker growth in a glass fiber while being drawn from the melt.

To summarize, then, UARL feels that the three types of microstructure demonstrated as existing in glass (Refs. 10 through 29) have not been considered in connection with the mechanical properties of such glasses even though studied in connection with other glass properties such as thermal expansion and electrical characteristics. It is proposed, therefore, that a basic investigation be carried out of the effect on mechanical properties such as elastic modulus and strength of

the three basic types of structure found in two-phase glasses, that is, colloidal or light-scattering structures which may be isolated droplets of a second phase or continuous interpenetrating two-phase structures, micellular or subcolloidal structures which may be isolated droplets or crystals, and two-phase glasses containing one component in the crystalline and the other in the vitreous state. It is clear that such structures must definitely affect the mechanical properties of such glasses even though no prior systematic investigation of this nature has been carried out. It is not obvious, however, whether such structures strengthen glasses and enhance their moduli or act conversely although preliminary investigations at UARL reported below indicate a favorable trend. Such an investigation cannot be dismissed as academic in connection with the enhancement of the properties of glass fibers since R. J. Charles (Ref. 15) has shown that borosilicate glasses such as Vycor and Pyrex are fully phase-separated when rapidly cooled from the melt. Since this is believed to be a typical spinodal decomposition, like results would be anticipated for all spinodal decompositions and, indeed, preliminary experiments with fibers drawn from UARL experimental glass 278, whose composition is given below, confirm that two-phase separation as the fiber is drawn is indeed possible.

To examine the possibilities of this type of approach, UARL has carried out a brief preliminary study in which five experimental two-phase glasses selected on the basis of a preliminary examination of the literature (Refs. 10 through 29) were melted, heat treated, examined by electron microscopic procedures, and in two cases Young's modulus was determined before and after heat treatment on circular rods formed by aspiration directly from the molten glass. The compositions of the five glasses are given in Table Ic in terms of the actual ingredients used in the batch.

The modulus contained for these glasses is shown in Table IV and summarized directly below

	<u>278</u>	<u>279</u>	<u>280</u>	<u>281</u>	<u>282</u>
Modulus (millions psi) as formed	13.29	11.96	5.56	6.42	5.14
Modulus (millions psi) after heat treatment	15.23	---	6.23	---	---
Reference for Composition	17	17	28	19	19

The results of the electron microscopic investigations of these glasses are shown in Figs. 1 through 14. For the most part, except where specifically noted otherwise, the electron micrographs are taken at 20,000 diameters and comprise platinum preshadowed carbon replicas of fresh fracture surfaces except for Fig. 6, which is a replica of an "as cast" surface. Parlodion was flowed over the surface immediately upon fracture so that atmospheric exposure was held to a minimum.

Figures 1 through 3 are of fracture samples of UARL glass 278. This glass and its companion glass, UARL 279, studied below were selected from an investigation originally carried out by Hummel, Tien, and Kim (Ref. 17) of the opaque white glasses that can be obtained in the systems $\text{Li}_2\text{O-TiO}_2\text{-SiO}_2$ and $\text{CaO-TiO}_2\text{-SiO}_2$ from the separation of immiscible liquids. Their work represents one of the early attempts to

exploit liquid opacification in place of the more usual practice of opacifying glasses, glazes, and enamels by the inclusion of gaseous or crystalline particles in the vitreous matrix. Figure 1 is an electron micrograph of a very dense opal glass successfully produced by liquid opacification incorporating droplets of a second immiscible glass in the first glass viewed as a vitreous matrix. This figure might well pass for the "classical" since 1956 phase separation photograph since it shows essentially only an abundance of droplets (spherical elevations) on an otherwise featureless background. Figure 2 is a fracture surface of the same glass after heat treatment at 800°C for ten hours. The glass is again a dense opal glass and the electron micrograph shows droplets of glass 2 now greatly increased in size again a background of glass 1 which has now undergone further decomposition as represented by the multitude of much smaller droplets present. In Fig. 3 the heat treatment has become sufficiently extended to produce lath-like crystals in a glassy matrix. The contrast of Fig. 1 with Fig. 2 would seem to confirm that phase separation of a second glass can enhance the modulus of the glass since, as noted in the table, glass 278 after heat treatment has a Young's modulus of 15.23 million psi in comparison to its original value of 13.29 million psi.

Figures 4 through 7 are concerned with UARL experimental glass 279. This glass, also taken from Hummel, et al (Ref. 17), is very different from 278. The substitution of zirconia for titania in the composition results in a glass which is transparent after melting and cooling to room temperature in place of the very dense opal of UARL 278. Figure 4 confirms the true transparency of this glass since even at the increased magnification of 30,000 the micrograph is essentially featureless, representing only a homogeneous glass. In Fig. 5, taken of a freshly fractured surface of this glass after heat treatment at 900°C for 3 hours, it will be noted that again true glass immiscibility has developed, as evidenced by the isolated droplets of glass 2 in the vitreous matrix of glass 1 and, indeed, the glass is again a dense opal. Figure 6, the micrograph not based on a fractured surface, shows the as-cast surface of glass 279 after heat treatment for 3 hours at 900°C. In Fig. 7, the complete crystallization present in the outside surface of the heat treated specimen has resulted in an oriented array of massive lath-form crystals.

Figures 8 and 9 are based on UARL glass 280, a Vycor-like composition selected by Watanabe, Noake, and Aiba (Ref. 28) for investigation. This glass has the usual composition of the Corning Vycor-glass before the second phase is reached. As melted, the glass forms a completely homogeneous glass, as evidenced by the featureless micrograph of Fig. 8. After heat treatment for 3 hours at 650°C, the glass has lost its pristine brilliance and now appears slightly opalescent. This opalescence is completely explained by Fig. 9, which shows that a second glass phase is now present in the form of very tiny droplets in contrast to the droplets of glasses 278 and 279. This phase is believed to be due to a spinodal-type decomposition. While the modulus of this glass, a high borosilicate, is very low, the phase-separable second glass again raises the value of Young's modulus from 5.56 million psi to 6.23 million psi.

Figures 10 and 11 are from UARL glass 281, which, together with UARL glass 282, is selected from a study by Levin and Cleek (Ref. 19) of the "Shape of Liquid Immiscibility Volume in the System Barium Oxide-Boric Oxide-Silica." The composition for UARL glass 281 is selected from those in the center of the spinodal decomposition region while that for 282 is on the edge of the dome. Glass 281, as melted and after cooling to room temperature, is a dense opal similar to 278. As can be seen from Fig. 10, a slight phase separation is apparent. After heat treatment at 900°C for 3 hours, it will be noticed from Fig. 11 that a marked growth of the isolated droplets of phase 2 has resulted.

Figures 12, 13 and 14 are based on glass 282. As already mentioned, this glass is chosen from the edge of Levin and Cleek's (Ref. 19) dome of spinodal immiscibility. As prepared, it is again a dense opal. The monstrous size of the separated liquid phase 2 is apparent in both Fig. 12 (7200X) and Fig. 13 (12,000X), as is the fact that we now have droplets in droplets in droplets. Figure 14 represents this glass after heat treatment for 3 hours at 650°C. Apparently the very large droplets have now gone into solution while the smaller droplets have continued to grow.

Elements present in Figs. 5, 10 and 11 resulting from the fractography process itself may best be understood from the work of Ohlberg, Golob and Hollabaugh (Ref. 20), who showed that the tail-like structures emanating from the dispersed phase are related to the crack front propagation and are affected by the relative values of the cohesive strength of the dispersed phase and the adhesive strength between the dispersed phase and the matrix. The appearance of a single tail emanating from the dispersed phase indicates that the cohesive strength of this phase is weaker than the adhesive strength at the droplet-matrix interface. A double tail emanating from a dispersed phase indicates its cohesive strength is greater than the adhesive strength between the matrix and the dispersed phase. Finally, if the dispersed phase is water soluble and special precautions are not taken, a fracture surface will evidence only depressions rather than the expected elevations and depressions characteristic of adhering droplets and complementary holes.

Methods Used in Preparing Selected Glasses

Just as in the case of our earlier experimental compositions, once a composition has been selected, 500 gram batches of the specified raw materials are melted in high purity (99.9%) alumina crucibles in air using kilns heated by Super-kanthal hairpin electrical resistance elements. Starting materials used are 5 micron particle size high purity silica, high purity alumina of 325 mesh, laboratory reagent grade magnesium oxide, 99.9% lanthanum oxalate, and other comparable materials such as reagent grade zinc carbonate or calcium carbonate. These materials customarily yield a water-white optical grade glass free of seed, stone and bubbles when properly compounded and held at temperatures of 1000-1650°C for at least two hours. Less commonly, glasses may be prepared in beryllia crucibles in air and in the same kilns, or in platinum crucibles in air in the

platform kiln which is heated by the high temperature variety of Super kanthal heating elements and can reach temperatures of 1700°C, or in tungsten crucibles in purified argon or vacuum atmospheres. Alumina crucibles of even very slightly lower purity, i.e. 99.3 to 99.7% have not proven useful for this type of glass research.

DIRECT OPTICAL OBSERVATIONS OF THE KINETICS OF GLASS CRYSTALLIZATION

Estimation of Liquidus and Working Range

The direct microscopic observation of the kinetics of crystallization of molten oxides as well as the direct measurement of their liquidus and the estimation of their working range is readily possible by means of a microfurnace and is invaluable in deciding which experimental glass compositions are likely to fiberize readily.

This UARL microfurnace design owes much to the earlier furnace constructed by Morley (Ref. 30) for exactly the same type research, namely, the study of crystallization kinetics in molten glass. The microfurnace consists essentially of a platinum-20% rhodium tube, 0.250 in. O.D. and with a wall thickness of 3 mils, which is clamped between the two copper bars (0.187 in. x 0.750 in.). A circular shelf of platinum is welded to the inside of the tube, and the crucible is placed in a 0.128 in. hole in this shelf. Crucibles are fabricated by cutting platinum tubing (0.125 in. dia with 5 mil wall thickness) into pieces 0.065 in. long and then pressing them in a die so that they form a 40-degree included angle.

Figure 15 shows the microfurnace without radiation shielding. Subsequently, radiation shielding was found necessary and was added by welding two rings of 0.057 in. Kanthal wire to the nichrome plates at the two ends of the heater tube. An inner shield of 4 mil platinum-rhodium sheet and an outer shield of 5 mil nichrome sheet were welded to the inner nichrome wire ring that is on the lower nichrome plate. Two 5 mil nichrome shields were welded to the outer nichrome wire ring on the upper circular nichrome plate.

Figure 15 also shows the 1/8 in. dia copper tubing which is used to supply water-cooling to the copper electrical connectors. The power supplied the furnace comes from a filament transformer of 0.975 KVA capacity and a 20 ampere Variac. To attain a temperature of 1400°C a current of 140 amperes at 1.1 volts (60 cycle a-c) has proven adequate.

The entire experimental arrangement with the exception of the power supply is shown in Fig. 16. It comprises the microfurnace, microscope and camera, micromanipulator used to weld and position the thermocouple, the x-y recorder used for plotting time-temperature response of the furnace, and the 3 mil

platinum-platinum 10% rhodium thermocouple carefully positioned in the center of the furnace. Experience has shown that the furnace temperature can be maintained to within $\pm 4^{\circ}\text{C}$ at 1250°C .

In actual use, the crucible is inserted into the furnace, a large fragment of glass is placed in the crucible and the crucible then heated. Smaller glass fragments are later added to completely fill the crucible. The glass is then heated until all of the bubbles disappear and then cooled to the temperature selected for crystal growth observation. The thermocouple is then lowered into the melt and photographs are taken of the crystals growing on the thermocouple at selected time intervals. Seed crystals can be grown on the thermocouple by placing it in the melt and then withdrawing it to a cooler part of the furnace, a step that may or may not be necessary, depending on the composition of the glass under investigation. High-speed film is used (Polaroid-ASA 3000) and good quality pictures are readily obtainable. The actual sizes of the crystals in the photographs can readily be obtained by calibrating the optical system employed.

During this report period, many of the new experimental glasses were characterized by optical examination in UARL's microfurnace. These characterizations essentially consisted of evaluating those properties of the glasses which are of importance in forming fibers. The properties consisted of the liquidus temperature, and the temperature at which the viscosities of the glasses were equal to 1000 and 100 poises. The rate of crystallization was also noted at a temperature of 50° below the liquidus temperature. This temperature was selected on the basis of our earlier examinations, which revealed that at such a temperature a fairly high rate of crystal growth would occur.

The liquidus temperature was determined by filling the crucible with the glass in the same manner as used in the determinations of the rate of crystal growth. The glass was heated until homogenized by convection currents, and then cooled to allow crystals to nucleate and grow to a few tens of microns in diameter. The crucible is then reheated until the crystals disappear, the temperature is noted and the process is then repeated until a satisfactory liquidus temperature is obtained. The viscosities of the experimental glasses were estimated by comparing their behavior when stirred with the thermocouple with that of a standard glass. "E" glass was used as the standard, and the viscosity versus temperature data of Tiede (Ref. 31) were used to obtain the temperatures at which the viscosity of E glass was 1000 and 100 poises. The viscosities which are estimated in this manner are not exact measurements, of course, but should be of value in drawing fibers of these glasses. The rates of crystal growth are also important in these glasses, and these were obtained by heating the glass above the liquidus temperature until all of the crystals were melted, and then lowering the temperature to 50° below the liquidus temperature and noting the rate of crystal growth which occurred in a 10 minute interval. This rate is reported in semiquantitative terms, such as slow, moderate, and rapid. A rapid

growth rate would be measured in hundreds of microns per minute and a slow rate would be measured in a few tens of microns per minute, or less.

The data thus collected are listed in tabular form in Table II. The upper temperature limit for the operation of the microfurnace has been arbitrarily set at 1540°C. This is because at temperatures appreciably higher than this, the lifetime of the platinum rhodium heater tubes is seriously decreased. Because of this temperature limitation, the temperature at which the viscosity equals 100 poises could not be determined for some of the experimental glasses. An examination of the data would indicate, for example, that UARL glasses 267, 275, 276, 286, 287, 290, 291, 292 and 294 should be readily fiberizable. Using the "poor man's" bushing described in the previous section experiment would indicate that fibers could readily be drawn at high rates of speed from 275, 276, 290, and 291. However, preliminary trials with 286, 287 and 294 were unsuccessful due to the high fluidity.

Role of Lanthana in Kinetics of Crystallization of UARL Cordierite Based Glasses

In the quarterly status reports, rates of crystal growth of cordierite have been presented as functions of temperatures for various glasses. The compositions of some of these glasses consist of MgO, Al₂O₃, and SiO₂, and in other glasses about 5 weight % of a rare earth-oxide. These glass compositions and the maximum rates of growth of cordierite are listed below:

<u>Batch</u>	<u>1</u>	<u>1-B</u>	<u>62</u>	<u>63</u>	<u>64</u>
wt % MgO	18.9	15.0	15.36	17.24	17.20
wt % Al ₂ O ₃	29.7	30.0	25.06	23.08	27.92
wt % SiO ₂	51.1	55.0	53.41	53.50	51.66
wt % R ₂ O ₃	0	0	5.6 Ce ₂ O ₃	5.6 La ₂ O ₃	3.12 Y ₂ O ₃
growth rate, max.	485	300	117	66	190

If these compositions are recalculated so as to consider only the MgO-Al₂O₃-SiO₂ ratios, the results are as listed below:

<u>Batch</u>	<u>1</u>	<u>1-B</u>	<u>62</u>	<u>63</u>	<u>64</u>
wt % MgO	18.9	15.0	16.3	18.3	17.8
wt % Al ₂ O ₃	29.7	30.0	26.7	24.6	28.8
wt % SiO ₂	51.0	55.0	57.2	57.1	53.3

It can be seen from these tabulations that the much lower rate of devitrification in batch 63 is not due to the high silica content, because batch 62 has nearly the same silica content, less magnesia and more alumina. Further, batch 1-B has similar MgO-Al₂O₃-SiO₂ ratios as does batch 63, but has a maximum rate of crystal growth of 300 microns per minute as compared to 66 microns per minute in batch 63. As a consequence

Table II

Liquidus Temperature and Working Characteristics of
Several UARL Invert Analog Glasses

<u>Sample No.</u>	<u>Liquidus Temperature</u>	<u>100 Poises</u>	<u>1000 Poises</u>	<u>Rate of Growth 50° below Liquidus Temperature</u>
102	1301	1474	1296	very slow
247	1292	1447	1153	slow
249	1256	1279	1176	slow
250	1447	>1500	1297	very slow
251	1330	1439	1314	slow
252	1405	>1500	1259	very slow
253	1510	>1500	1376	rapid
256	1447	>1500	1338	rapid
257	1464	>1500	1407	rapid
265	1435	>1500	1372	rapid
267	1390	>1500	1281	very slow
273	1435	1470	1340	moderate (2 types)
275	1322	>1500	1281	slow
276	1346	1498	1272	no crystals
285	1276	1443	1243	moderate
286	1343	1422	1297	no crystals
287	1158	1473	1276	no crystals
290	1220	1440	1280	no crystals
291	1231	1414	1247	no crystals
292	1260	1385	1156	slow
293	1290	>1500	1372	rapid
294	1414	1473	1291	no crystals
295	1185	1426	1206	no crystals
296	1310	1431	1227	no crystals
299	1206	1406	1174	no crystals
300	----	1268	1055	no crystals
311	1475	>1500	1410	few crystals
316	1435	1477	1310	few isolated crystals
318	1490	>1500	1443	no crystals
319	1515	1495	1290	moderate to slow
322	1500	1435	1290	no crystals
325	1444	1322	1481	few large crystals
331	1483	1456	1381	rapid
335	1490	1510	1380	moderate

of these observations it was decided to use the electron microprobe to determine if the mechanism by which the devitrification rate is so altered could be found. Specifically, it was desired to determine if the large lanthanum ions in batch 63 could be incorporated into the cordierite crystals in any manner and, if not, to determine if the lanthana would be concentrated in an area surrounding that part of the crystal which is growing the fastest. Accordingly, a sample of glass from batch 63 was placed in a crucible in the microfurnace, and a cluster of hollow cordierite crystals (Fig. 17a) were grown at a temperature of $1290 \pm 5^\circ\text{C}$, which corresponds to a rate of growth of about 5 microns per minute. The crucible was then removed from the microfurnace, embedded in bakelite, and then sectioned and polished so that the crystals were exposed on the polished surface. In order to be certain that the crystals were exposed on the polished surface, it was necessary to etch the sample (as shown in Fig. 17b), and then repolish it for the electron microprobe analysis.

This specimen preparation is necessary because the electron microprobe analyzer can sample the specimen only to a depth of about two microns. The microprobe utilizes a high energy (20 kv) electron beam which can be focused to a spot one micron in diameter on the surface of the specimen. This spot can be viewed with an optical microscope so that the specimen can be analyzed in the desired area. The high energy electrons impinging upon the specimen cause the constituent elements to emit characteristic X-rays. These X-rays may be analyzed with respect to wavelength and intensity to yield spectra from which qualitative and quantitative analyses may be made. This is accomplished by diffracting the X-rays with a crystal and measuring them with an appropriate detector. The output of the detector is channeled through electronic signal processing equipment to a strip chart recorder. The record from the strip chart recorder thus contains peaks whose location and amplitude are proportional to the elements present in the sample. By tuning the spectrometer to a specific spectral line, sweeping the beam across the sample and displaying the detector output on an oscilloscope, a picture of the elemental distribution can be shown. This can then be photographed to provide a permanent record, as shown in Figs. 18a and 18b for lanthanum and aluminum. Specimen current images may also be photographed from the oscilloscope. In this measurement, that portion of the electron beam which penetrates into the sample gives rise to a current flow which is proportional to the atomic number of the elements upon which the beam is impinging. In this measurement, the darker areas are composed of elements having a lower atomic number than are the lighter areas, as shown in Figs. 18a and 18b. The electron microprobe analyses of the cordierite crystals grown in batch 63 consisted of specimen current, lanthanum X-ray, and aluminum X-ray images which were recorded on polaroid film, and lanthanum distribution scans across selected areas which provided a more accurate measurement of the lanthanum distribution than could be obtained from the pictorial representation. The paths which were scanned are shown in Fig. 19 and the scans are shown in Figs. 20a, b, c, d, e, and f.

The specimen current images show that the elements comprising the crystals are of lower atomic numbers than the elements constituting the matrix. This is

because the crystals contain more alumina and silica and less magnesia than does the glass matrix, and also because, as shown in Fig. 18a, the crystals contain very little, if any, lanthanum. Figures 18a and 18b also show the enrichment in aluminum in the crystals as compared to the glass matrix. The area shown in Fig. 18b is the area in which scans were made in order to determine the lanthanum distribution, and Fig. 19 is a schematic representation of the paths scanned by the electron beam so as to get the distribution of lanthanum in and surrounding the crystals. Figure 19 is drawn accurately with respect to scale so that the separation between scans is 12.7 microns. The scans were concentrated near the end of the hollow crystal, which was, of course, the area where the fastest rate of growth was occurring. The results of the scans are shown in Figs. 20a, b, c, d, e, and f. Scans 1 and 2 in Fig. 20a show that the crystal contains very little, if any, lanthanum while the center portion is enriched in lanthanum up to about 7 or 8 wt %. Scan 3 contains only one side of the crystal, and shows about 7 or 8 wt % La_2O_3 immediately adjacent to the crystal and a linearly decreasing amount as the beam scanned out into the matrix. The distance scanned by the beam from the edge of the crystal to the end of the scan is about 60 microns, which means that the beam passed by the end of the other side of the crystal about 3 microns away from the end, without showing any increase in the concentration of lanthanum. Scan 4 is nearly the same as scan 3, and shows about 7-8 wt % La_2O_3 very near the tip of the crystal which decreases linearly away from the crystal edge. Scans 5 and 6 show no variation in the La_2O_3 content throughout the scan.

The results show that the lanthanum is diffusing away from the crystal-glass interface at the ends of the growing crystal and that if a lanthanum enriched zone is present, it is less than one micron in thickness. The analyses do show that there is a lanthanum enriched zone within the hollow portion of the crystal, in which the only diffusion path is toward the open end of the crystal. The mechanism by which the lanthanum ion alters the rate of crystal growth may be an adsorption of lanthanum ions on the growing crystal face, and apparently is not due to a thicker lanthanum enriched zone within the glass.

CHARACTERIZATION OF EXPERIMENTAL GLASSES BASED ON BULK SPECIMENS

Density Measurements

Density of the experimental glasses has been determined for UARL by the Glass Testing Laboratory of the Hartford Division of the Emhart Corporation. For samples with densities less than 3.00 gms/cm^3 the heavy-liquid of known density comparison procedure was used while for samples with densities greater

than 3.00 gms/cm³ the Archimedean method served. The results of density measurements are shown in Table III. The observed densities range from 2.57 to 5.22 gms/cm³. Noteworthy is the density for a copper containing glass such as number 284 where a partial substitution of copper for zinc lowers the density from 3.52 gms/cm³ to 3.23 gms/cm³. Again for glass 286 the substitution of 10 mol % B₂O₃ for an equal molar percentage of SiO₂ raises the density from 3.7271 gms/cm³ (glass 257) to 3.7951 gms/cm³ while the substitution of 5 additional molar percent of B₂O₃ (glass 285) results in partial devitrification and lowers the density to 3.6569 gms/cm³.

Young's Modulus for Glass Rods Aspirated Directly from Melt

Samples for modulus measurement are prepared using the simple and inexpensive technique of drawing samples directly from the crucibles of molten glass into fused silica tubes previously dusted lightly with powdered magnesia. Controlled suction for pulling the sample into the fused silica tube, is supplied by a hypodermic syringe. The fact that most glasses have higher thermal expansion coefficients than the fused silica results in the shrinking of the drawn bar away from the silica tube on cooling to room temperature allowing the ready recovery of the sample. Since the rods drawn in this manner represent a glass of higher fictive temperature than the former procedure employed at UARL when the samples were prepared by precision machining from massive cast and annealed slabs, the results are not directly comparable with the earlier results reported for bulk samples.

All data available for modulus determinations on glass rods pulled directly from the melt is shown in Table IV. Comparative data are supplied on rods prepared from Owens-Corning Fiberglass Corporation "E" glass marble, glass 83 prepared from the teachings of example 4 of Tiede's U.S. Patent 3,122,277 and Schott Optical Glasses SFS1, SF6, LaSF3, LaSF6. In direct comparison with these known materials are the values for UARL's experimental glasses, it will be noted that experimental glasses 231, 233, 270, 325, and 329 have values for Young's modulus greater than 20 million psi while glasses 233, 273, 323, and 329 have specific moduli of 6.5 or greater expressed in hybrid units (millions of psi per gm per cubic centimeter).

The extent to which the data of Table IV can be relied on as well as some precautions in its interpretation is best shown by an examination of Table V which shows the reproducibility of individual determinations of Young's modulus on rods pulled directly from the melt. It will be noted that the reproducibility of this is high, for example, for sample 257 the individual values are 17.85, 18.65, 18.28, 17.43, 18.28, 16.82, 17.88, 18.97 and 18.47 for an average value of 18.35 million psi or for sample 288 - 14.27, 14.48, 14.14, 13.99, 14.49, and 14.42 for an

Table III

Summary of all Density Determinations for Bulk Specimens
of UARL Experimental Glasses

<u>Number</u>	<u>Density</u> <u>gms/cm³</u>	<u>Number</u>	<u>Density</u> <u>gms/cm³</u>	<u>Number</u>	<u>Density</u> <u>gms/cm³</u>	<u>Number</u>	<u>Density</u> <u>gms/cm³</u>
25	2.5672	125	2.7818	194	4.479	258	2.7232
38	2.6415	126	3.4634	195-2	4.167	259	2.8988
40-3	2.9574	127	3.2557	200	3.584	260	2.6191
56	2.4368	131	3.1386	201	3.550	261	2.5783
62-3	2.7404	134	3.0671	202	3.769	262	2.3180
63-1	2.6847	135	2.6303	203	3.490	263	4.0091
64-1	2.6818	136	2.8035	205	4.0576	265	3.9818
65-1	2.7197	137	3.0834	210	3.8972	266	3.1872
66	2.6112	138	3.5498	212	3.0360	267	2.7162
66-1	2.6784	140	3.678	214	2.5854	268	3.1986
67-3	2.6499	151	3.2541	215	3.1277	269	3.4357
68-2	2.6295	155	3.5452	219	2.9689	270	3.5259
69	2.5910	157	2.6962	222	4.4871	271	3.7692
69-3	2.5952	159	3.2216	223	5.2235	273	2.7472
70-1	2.7526	160	3.2211	224	5.1584	274	2.9926
71	2.6627	161	3.4523	225	4.6850	275	3.6460
72-2	2.8877	162	3.6150	231	3.4337	276	3.3983
73-2	3.0152	163	3.1876	232	3.5892	277	3.9086
74	2.9983	164	4.0593	233	3.0314	278	2.6073
75	2.6342	165	3.3088	234	3.7081	279	2.6941
82-3	2.5875	166	2.6295	235	3.3261	280	2.0556
83	2.8376	167	3.4085	237	3.3335	281	2.4152
93	3.1167	168	3.2047	238	3.0462	282	2.2126
96	2.9676	169	3.6355	244	3.63	283	3.6391
97	2.8426	170	4.202	247	2.9870	284	3.3233
98	2.9168	171	3.810	248	3.0906	285	3.6569
99	3.186	172	3.934	249	3.0114	286	3.7951
102	2.9188	173	4.525	250	4.3226	287	3.6206
103	2.9089	174	3.472	251	3.0660	288	3.6110
106	3.6859	175	3.189	252	3.0680	289	3.9026
107	3.3799	176	3.151	253	3.2534	290	3.2423
108	3.1140	177	4.196	254	3.6307	291	3.3225
110	2.6128	178	3.613	255	4.1231	292	3.6614
113	3.5298	179	4.331	256	3.5838	293	3.2873
114	3.2237	188	3.2548	257	3.7271	294	3.3745

Table III (Cont'd)

<u>Number</u>	<u>Density</u> <u>gms/cm³</u>
295	3.1942
296	3.2892
297	3.5426
298	3.9706
299	3.1904
300	2.8883
301	3.8131
302	3.7684
303	3.7256
304	3.6248
305	3.6629
306	3.6654
307	3.6950
308	3.5651
309	3.5951
310	3.6864
311	3.7008
312	3.2789
314	3.7178
315	3.5831
316	3.8017
317	3.8051
318	2.7173
319	3.6270
320	2.9286
321	3.6319
322	2.9967
323A	2.7711
324A	2.9708
325A	3.5446
326	3.0939
327	3.6914
328	4.3740
329	3.0380
330	
331	3.6638
332	4.2390
333	3.7066
334	
335	

Table IV

Summary of All Values for Young's Modulus Measured on
Circular Rods Formed Directly from Melt

Glass Number	Density gms/cm ³	Young's Modulus 10 ⁶ psi	Specific Modulus 10 ⁶ psi/gms/cm ³	Glass Number	Density gms/cm ³	Young's Modulus 10 ⁶ psi	Specific Modulus 10 ⁶ psi/gms/cm ³	Glass Number	Density gms/cm ³	Young's Modulus 10 ⁶ psi	Specific Modulus 10 ⁶ psi/gms/cm ³
38	2.6415			136 ^a	2.8035	14.4	5.13	236 ^a	---	---	---
40-3 ^a	2.9574	15.5	5.24	137 ^a	3.0834	13.3	---	237	3.3335	18.3	---
62-3 ^a	2.7404	14.18	5.18	138 ^a	3.5498	15.3	4.32	238	3.0462	---	---
67-3 ^a	2.6499	14.43	5.44	140 ^a	3.678	15.6	4.23	239 ^a	---	---	---
68-3 ^a	2.6295	14.1	5.4	155 ^a	3.5452	15.7	4.43	240 ^a	---	---	---
69-3 ^a	2.5952	14.16	5.47	157 ^a	2.6962	13.3	4.93	241 ^a	---	---	---
72-2 ^a	2.8877	14.0	4.8	159 ^a	3.2216	16.2	5.03	247 ^b	2.9870	15.07	5.03
83	2.8376	16.0	5.63	166 ^a	2.6295	12.53	4.77	248 ^b	3.0906	15.71	5.08
96	2.9676	15.7	5.28	174 ^a	3.472	---	---	249 ^b	3.0114	15.86	5.23
99 ^b	3.186	10.5	3.29	175 ^a	3.189	---	---	250 ^b	4.3326	14.83	3.43
102 ^b	2.9188	15.04	5.16	176 ^a	3.151	---	---	251 ^b	3.0660	15.86	5.17
108 ^b	3.1140	14.81	4.77	179 ^a	4.331	14.9	3.44	252 ^b	3.0680	14.87	4.83
114 ^a	3.2237	16.7	5.18	194	4.479	14.7	3.28	253 ^b	3.2534	12.28	3.77
125 ^a	2.7818	16.14	5.81	219	2.9689	14.8	4.98	256 ^b	3.5838	17.88	5.00
126 ^a	3.4634	16.8	4.86	222	4.4871	14.8	3.30	257 ^b	3.7271	18.35	4.92
127 ^a	3.2557	16.13	4.94	231 ^a	3.4337	20.12	5.86	258	2.7232	13.5	4.97
129 ^a	3.3105	16.5	4.98	232 ^a	3.5892	18.09	5.04	259	2.8988	13.24	4.57
131 ^a	3.1386	14.00	4.47	233 ^a	3.0314	22.36	7.38	263 ^a	4.0091	14.49	3.54
134 ^a	3.0671	15.4	5.02	234 ^a	3.7081	18.05	4.87	265 ^b	3.9818	16.28	4.09
135 ^a	2.6303	14.3	5.43	235 ^a	3.3261	---	---	266 ^b	3.1872	16.73	5.25
110 ^a	2.6128	14.62	5.60								

Table IV (Cont'd)

Glass	Number	Density gms/cm ³	Young's Modulus 10 ⁶ psi	Specific Modulus 10 ⁶ psi/gms/cm ³	Glass	Number	Density gms/cm ³	Young's Modulus 10 ⁶ psi	Specific Modulus 10 ⁶ psi/gms/cm ³	Glass	Number	Density gms/cm ³	Young's Modulus 10 ⁶ psi	Specific Modulus 10 ⁶ psi/gms/cm ³	Glass	Number	Density gms/cm ³	Young's Modulus 10 ⁶ psi	Specific Modulus 10 ⁶ psi/gms/cm ³	Glass	Number	Density gms/cm ³	Young's Modulus 10 ⁶ psi	Specific Modulus 10 ⁶ psi/gms/cm ³	Glass	Number	Density gms/cm ³	Young's Modulus 10 ⁶ psi	Specific Modulus 10 ⁶ psi/gms/cm ³		
267 ^b		2.7162	15.34	5.65	282		2.2126	4.80	2.17	304 ^a		3.6248	19.23	5.31	3.6248		3.6248	19.23	5.31	5.31	304 ^a		3.6248	19.23	5.31	5.31	304 ^a		3.6248	19.23	5.31
268 ^b		3.1986	16.93	5.29	282 ^{c, d}		2.2126 ^d	6.22 ^d	2.82 ^d	305 ^a		3.6629	17.72	4.83	3.6629		3.6629	17.72	4.83	4.83	305 ^a		3.6629	17.72	4.83	4.83	305 ^a		3.6629	17.72	4.83
269 ^b		3.4357	17.18	4.99	283 ^b		3.6391	15.47	4.24	306 ^a		3.6654	18.85	5.13	3.6654		3.6654	18.85	5.13	5.13	306 ^a		3.6654	18.85	5.13	5.13	306 ^a		3.6654	18.85	5.13
270 ^b		3.5259	20.25	5.73	284 ^b		3.3233	14.85	4.47	309 ^b		3.5951	16.86	4.70	3.5951		3.5951	16.86	4.70	4.70	309 ^b		3.5951	16.86	4.70	4.70	309 ^b		3.5951	16.86	4.70
273-1 ^b		2.7472	18.39	6.68	285 ^b		3.6569	15.07	4.12	310 ^b		3.6864	16.66	4.53	3.6864		3.6864	16.66	4.53	4.53	310 ^b		3.6864	16.66	4.53	4.53	310 ^b		3.6864	16.66	4.53
273-2 ^b		2.7472	17.2	6.27	286 ^b		3.7951	15.60	4.12	311 ^b		3.7008	15.90	4.30	3.7008		3.7008	15.90	4.30	4.30	311 ^b		3.7008	15.90	4.30	4.30	311 ^b		3.7008	15.90	4.30
274 ^b		2.9926	17.23	5.77	287 ^b		3.6206	15.14	4.18	312 ^b		3.2789	16.52	5.03	3.2789		3.2789	16.52	5.03	5.03	312 ^b		3.2789	16.52	5.03	5.03	312 ^b		3.2789	16.52	5.03
275 ^b		3.6460	16.67	4.57	288 ^b		3.6110	14.30	3.96	313 ^b		-----	-----	-----	-----		-----	-----	-----	-----	313 ^b		-----	-----	-----	-----	313 ^b		-----	-----	-----
275 ^b		3.6460	16.80	4.62	289 ^b		3.9026	14.95	3.83	314 ^b		3.7178	16.99	4.57	3.7178		3.7178	16.99	4.57	4.57	314 ^b		3.7178	16.99	4.57	4.57	314 ^b		3.7178	16.99	4.57
275 ^b		3.6460	-----	-----	290 ^b		3.2423	14.52	4.48	315 ^b		3.5831	16.63	4.63	3.5831		3.5831	16.63	4.63	4.63	315 ^b		3.5831	16.63	4.63	4.63	315 ^b		3.5831	16.63	4.63
275 ^b		-----	-----	-----	291 ^b		3.3225	15.67	4.72	316 ^b		3.8017	16.46	4.33	3.8017		3.8017	16.46	4.33	4.33	316 ^b		3.8017	16.46	4.33	4.33	316 ^b		3.8017	16.46	4.33
275 ^b		-----	-----	-----	292 ^b		3.6614	15.36	4.19	317 ^b		3.8051	16.33	4.29	3.8051		3.8051	16.33	4.29	4.29	317 ^b		3.8051	16.33	4.29	4.29	317 ^b		3.8051	16.33	4.29
276 ^b		3.3983	15.82	4.66	293 ^b		3.2873	15.96	4.84	318 ^b		2.7173	15.97	5.87	2.7173		2.7173	15.97	5.87	5.87	318 ^b		2.7173	15.97	5.87	5.87	318 ^b		2.7173	15.97	5.87
277 ^b		3.9086	17.91	4.58	294 ^b		3.3745	17.62	5.23	319 ^a		3.6270	17.9	4.93	3.6270		3.6270	17.9	4.93	4.93	319 ^a		3.6270	17.9	4.93	4.93	319 ^a		3.6270	17.9	4.93
278		2.6073	13.29	5.09	295 ^b		3.1942	15.22	4.77	320 ^a		2.9286	15.96	5.44	2.9286		2.9286	15.96	5.44	5.44	320 ^a		2.9286	15.96	5.44	5.44	320 ^a		2.9286	15.96	5.44
278 ^{c, d}		2.6073 ^d	15.23 ^d	5.83 ^d	296 ^b		3.2892	16.53	5.03	321 ^a		3.6316	25.92 ^d	5.16	3.6316		3.6316	25.92 ^d	5.16	5.16	321 ^a		3.6316	25.92 ^d	5.16	5.16	321 ^a		3.6316	25.92 ^d	5.16
279		2.6941	12.35	4.58	297 ^b		3.5426	17.08	4.82	322 ^b		2.9967	21.94 ^d	5.64	2.9967		2.9967	21.94 ^d	5.64	5.64	322 ^b		2.9967	21.94 ^d	5.64	5.64	322 ^b		2.9967	21.94 ^d	5.64
280		2.0556	5.56	2.75	299 ^b		3.1904	14.57	4.57	323 ^b		2.7711	18.42	6.67	2.7711		2.7711	18.42	6.67	6.67	323 ^b		2.7711	18.42	6.67	6.67	323 ^b		2.7711	18.42	6.67
280 ^{c, d}		2.0556 ^d	6.23 ^d	3.04 ^d	300 ^b		2.8883	14.45	5.01	324 ^b		2.9708	17.78	5.98	2.9708		2.9708	17.78	5.98	5.98	324 ^b		2.9708	17.78	5.98	5.98	324 ^b		2.9708	17.78	5.98
281		2.4152	6.77	2.81	302 ^b		3.7684	17.16	4.56	325 ^b		3.5449	20.19	5.68	3.5449		3.5449	20.19	5.68	5.68	325 ^b		3.5449	20.19	5.68	5.68	325 ^b		3.5449	20.19	5.68

Table IV (Cont'd)

Glass Number	Density gms/cm ³	Young's Modulus 10 ⁶ psi	Specific Modulus 10 ⁶ psi/gms/cm ³	Glass Number	Density gms/cm ³	Young's Modulus 10 ⁶ psi	Specific Modulus 10 ⁶ psi/gms/cm ³
326 ^b	3.0939	16.98	5.87	346 ^b			
327 ^b	3.6914	18.36	4.98	347 ^b			
328 ^b	4.3740	---	---	348 ^b			
329 ^b	3.0380	20.7	6.82	349 ^b			
330 ^b	---	---	---				
331 ^b	3.6638			SFS1	6.98		
332 ^b	4.2390			SF6	5.18	6.91	1.33
333 ^b	3.7066			LaSF3	4.90	13.34	2.72
334 ^b				LaSF6	6.13	17.42	2.84
335 ^b				E	2.55	12.2	4.78

336^b337^b338^b339^b340^b341^b342^b343^b344^a345^a^aCordierite base^bInvert analogue^cValue after heat treatment^dPartially crystallized samples

Table V

Reproducibility of Values of Young's Modulus Measured
on Rods Aspirated Directly from Melt

Glass No.	Individual Determinations(10 ⁶ psi)				Average Modulus (10 ⁶ psi)	
40-3	15.6	15.1	15.6	15.5	15.5	
62-3	13.59	14.77	----	----	14.18	
67-3	14.5	14.6	14.24	----	14.43	
68-3	14.4	13.8	13.7	14.6	14.1	
69-3	14.11	14.37	14.00	----	14.16	
72-2	14.4	13.9	13.8	----	14.0	
83	16.0	16.0	16.0	16.0	16.0	
96	15.8	15.9	15.7	15.5	15.7	
99	10.7	10.5	10.4	10.5	10.5	
102	15.00	14.97	14.61	15.13	15.50 15.04	
108	14.79, 14.67, 14.84, 14.68, 14.69, 15.16				14.81	
110	14.69	14.07	14.73	14.99	14.62	
114	16.4	16.7	16.8	16.7	16.7	
125	16.2	15.8	16.2, 16.2, 16.3		16.14	
126	16.5	17.1	16.7	----	16.8	
127	15.49, 16.10, 16.51, 16.06, 15.81, 16.75				16.13	
129	16.9	16.1	16.3	16.6	16.5	
131	13.99	13.66	13.93	13.80	14.61 14.00	
134	15.3	15.4	----	----	15.4	
135	14.6, 14.5, 14.6, 14.0, 14.6, 14.3, 14.2				14.3	
136	14.6	14.2	14.4	----	14.4	
137	13.3	13.6	13.3	13.0	13.3	
138	15.3	15.2	15.4	15.3	15.3	
140	15.1	15.7	15.5	16.2	15.6	
155	15.6	15.7	15.7	15.7	15.7	
157	13.3	13.6	13.3	13.0	13.3	
159	16.5	15.9	16.0	16.4	16.2	
166	12.9	12.1	12.6	----	12.53	
179	14.6	14.8	14.6	14.9	14.7	
194	14.0	14.9	14.6	15.2	14.7	
219	14.87	14.65	14.87	----	14.80	
222	15.3	15.0	14.2	----	14.8	
231	20.37	20.26	18.63, 21.43, 19.08, 20.95		20.12	
232	20.11	17.10	17.46	17.87	18.09 18.13	
233	21.68	25.61	26.59	20.34	17.58 22.36	
234	17.95	17.87	18.14	18.22, 17.95, 18.16		18.05
237	18.00, 17.99, 18.43, 18.47, 18.61, 18.36, 16.93				18.16	
247	15.0	15.2	15.0	----	15.07	
248	20.5	16.0	15.42	14.03	16.48	
249	15.9	15.6, 16.0, 16.0, 15.8			15.86	
250	14.35	14.86	15.27	14.82	14.83	
251	16.08	15.48	16.05	15.82	15.86	
252	14.65	15.32	14.63	----	14.87	

Table V (Cont'd)

Glass No.	Individual Determinations (millions psi)					Average Modulus (millions psi)
253	12.28					12.28
256	17.35, 17.40, 18.05, 17.10, 17.68, 15.95, 17.70, 18.30, 17.92, 17.78					17.88
257	17.85, 18.65, 18.28, 17.43, 17.95, 18.28, 16.82, 17.88, 18.97, 18.47					18.35
258	13.5					13.5
259	13.08	13.21	14.0	12.67		13.24
263	14.85	14.22	15.08	14.30	14.00	14.49
265	16.58	16.68	16.17	15.67		16.28
266	16.62	16.97	17.12	16.22		16.73
267	14.62	15.70	15.40	15.6		15.34
268	17.00	17.03	16.75	----		16.93
269	17.8	17.1	16.95	16.85		17.18
270-2	20.2	20.8	19.9	20.1		20.25
273-2	16.57	17.73	17.88	17.80	17.35, 17.4	-----
273-1	----	----	17.90	18.28	18.97	18.39
273-D	17.25	17.13	17.38	17.90	16.23	17.18
274	21.2, 17.3, 18.42, 18.32, 17.75, 17.57, 16.48, 17.47, 16.70, 18.25					17.23
275-0	16.48, 16.64, 16.52, 16.65, 17.21, 16.54					16.67
275	16.65	17.21	16.54			16.80
276	15.47	15.0	15.82	16.48	16.32, 15.82	15.82
277-2	17.43, 17.43, 17.55, 18.32, 18.66, 17.93, 17.57, 17.80, 17.43					17.91
283	15.58, 15.36, 15.20, 15.62, 15.62, 15.39, 15.67					15.47
284	14.08, 14.87, 15.33, 15.07, 14.87					14.85
285	15.13, 15.31, 15.0, 15.17, 14.91, 14.89					15.07
286	16.86, 15.48, 14.81, 15.64, 15.49, 15.28, 16.46					15.60
287	14.53, 15.50, 14.79, 14.65, 15.26, 15.63					15.14
288	14.27, 14.48, 14.14, 13.99, 14.49, 14.42					14.30
289	14.74, 14.75, 15.19, 15.21, 14.86					14.95
290	14.47, 14.27, 14.72, 14.26, 14.50, 14.89					14.52
291	16.12, 15.32, 15.96, 15.67, 15.59, 15.37					15.67
292	15.46, 15.08, 15.73, 15.17, 14.78, 15.77					15.36
293	16.28, 16.15, 17.18, 14.93, 15.30, 15.86, 16.04					15.96
294						17.62
295						15.22
296	16.709, 15.12, 18.51, 15.49, 16.47, 16.87					16.53
297	17.174, 17.998, 18.082, 16.996, 16.483, 16.749					17.08
299	14.74, 14.35, 14.60, 14.63, 14.84, 14.28					14.57
300	14.36, 14.40, 14.58, 14.58, 14.47, 14.22, 14.68					14.45
302	17.23, 16.73, 17.58, 17.24, 17.04					17.16
304	24.06, 18.53, 18.45, 18.30, 19.12, 18.21, 17.91					19.23
305	17.1, 18.1, 17.7, 17.8, 17.9, 16.8					17.72

Table V (Cont'd)

Glass No.	Individual Determinations (millions psi)	Average Modulus (millions psi)
306	18.8, 18.9, 18.6, 18.7, 19.4, 18.7	18.85
309	16.92, 16.43, 16.91, 18.12, 16.59, 16.21	16.86
310	16.04, 19.58, 16.59, 15.88, 16.20, 15.65	16.66
311	16.31, 14.71, 14.98, 15.98, 16.49, 16.91	15.90
312	17.26, 15.81, 16.77, 16.25	16.52
314	16.39, 17.23, 16.68, 17.07, 17.19, 17.47, 16.89	16.99
315	16.89, 17.04, 16.17, 16.97, 16.14	16.63
316	16.55, 16.57, 16.18, 16.37, 16.52, 16.26, 16.39	16.46
317	15.84, 16.32, 16.87, 16.78, 16.64, 15.53	16.33
318	15.26, 15.68, 18.08, 15.91, 15.57, 15.44	15.97
319A	17.9, 18.02, 17.83	-----
319	15.96, 15.03, 15.86, 15.26, 15.01	15.42
320A	16.05, 15.98, 15.90, 16.12, 15.72, 16.00	15.96
320B	17.23, 19.33, 16.32, 16.31, 16.23, 16.79	17.03
321A	18.20, 17.92, 19.83, 18.09, 18.97, 19.07	18.7
322	17.56, 16.85, 17.18, 17.11, 16.71	17.08
322A	18.52, 18.11, 18.63, 18.72, 19.76, 18.87	18.60
323A	18.57, 18.14, 17.92, 20.05, 18.05, 17.79	18.42
324A	18.04, 17.99, 17.41, 17.25, 18.35, 17.62	17.78
325A	18.92, 19.75, 20.16, 21.17, 20.59, 20.55	20.19
325	19.82, 19.09, 19.05, 18.97, 19.87, 20.12	19.49
326A	16.53, 17.28, 17.05, 17.23, 16.79	16.98
326	16.89, 16.68, 17.83, 15.62	16.76
327	18.69, 17.99, 17.88, 18.34, 18.88	18.36
328		
329	20.68	20.68
E	12.42, 12.64, 12.14, 12.06, 11.98, 11.93	12.2
LaSF6	17.28, 17.23, 17.63, 17.55	17.42
LaSF3	13.08, 13.55, 13.72, 13.01	13.34
SFS1	7.18, 6.74, 7.06, 6.92	6.98
SF6	7.34, 6.90, 6.58, 6.82	6.91

average of 14.30 million psi. Accordingly when values as discordant as the first value of 21.2 for 27⁴ which has an average Young's modulus of 17.23 million psi or 24.06 for glass 30⁴ whose average value is 19.23 million psi are found, it can usually be shown that the discrepancy arises from a pronounced degree of crystallization present in the sample and such values could, therefore, safely be discarded.

FIBERIZABILITY STUDIES

Young's Modulus for Mechanically Drawn Experimental Glass Fibers Evaluated by Mechanical Tests

As described in our earlier reports F910373-7, F910373-8, F910373-9, G910373-10, and G910373-11, UARL prepares mechanically drawn fibers by the use of a "poor man's bushing". The bushing consists of a 20 cm³ platinum crucible with reinforced bottom and central hole which is formed by starting with a normal platinum crucible and welding several thicknesses of platinum foil to the bottom until a bottom thickness of 3/16 in. is obtained and then taper reaming a central orifice 0.088 in. at top, 0.063 in. at bottom and 3/16 in. long in bottom of crucible. The crucible is then filled with glass and introduced into the platform furnace with high temperature Super-kanthal hairpin heating elements (furnace temperatures in excess of 1700°C are obtainable) together with a ring orifice providing water cooling immediately below the crucible as well as a second ring orifice for cooling the fiber as it forms with helium jets. The equipment has now been extensively used and has proven satisfactory for the production of very nearly circular glass fiber having approximately one mil diameter at pulling rates of 4000 to 8000 ft/min.

Experimental glass fibers prepared as described above are evaluated for UARL by the Lowell Institute of Technology. Lowell Institute of Technology uses an Instron CRE tester operated with a machine speed of 0.2 in. per minute, a chart speed of 20 in. per minute, a gage length of 5 in., and a full scale capacity of 1.0 lb. The specimens were held in air actuated clamps with flat rubber coated faces.

For each fiber for which we give results in the table, a minimum of 20 specimens were taken from approximately the center portion of each spool. The specimens were 8 in. long with about one yard of fiber being discarded between each specimen. It was not always possible to select fibers in exactly this manner because many of the spools had discontinuous odd lengths of fiber, but in general, the specimens selected represent the middle 20 yds of the fiber supplied for testing. Three fiber diameter measurements were made in the middle three-inch

portion of each eight-inch specimen. These measurements were made using a monocular microscope equipped with an eyepiece reticule and operated with a magnification of 774 (18x eyepiece, 43x objective). Each reticule division was equal to 0.092 mils.

The average of the twenty determinations for each fiber is shown in Table VI together with the standard deviation for most of the fibers tested. In our earlier report F910373-8 it was shown in detail that the standard deviation for glass 126 was 1.82 million psi so that one could say with 99% probability that the tabulated average value of 16.4 million psi for this glass actually lies between 15.2 and 17.6 million psi. This degree of reproducibility or slightly worse may be ascribed to most of the fiber data entered in this table. It will be noted, however, that a few of the glasses such as 275, 276, 176, and 237 show a very much larger standard deviation.

Glasses 176, 237, 275, and 276 showed not only a much larger standard deviation than normal but in some cases showed individual modulus determinations greater than thirty million psi. The urgent question was whether any significance could be attached to these phenomenally high moduli. For example, had we developed a second phase in the glass during the drawing process, crystalline or second-glass, which could account for such values of moduli. Because of the importance of this question, much time was spent in the twelfth quarter seeking the answer to this question. The very first approach was to attempt to reduce the experimental scatter but greatly increasing the number of tests. The worst offender was obviously UARL 275. Here, increasing the number of tests from twenty to one hundred not only failed to decrease the standard deviation but yielded 42 determinations with values in excess of twenty million psi.

The next attempt to determine the significance of these high standard deviations and the accompanying excessively high values for Young's modulus consisted of attempting to correlate the range in diameter of fiber tested with the standard deviation for this fiber. Typical results of this investigation are shown in Table VII. It is immediately obvious that no correlation between standard deviation in diameter and/or range of diameter and standard deviation in Young's modulus exists.

Next approach was to consider that we had again encountered non-circular fibers of the type which had given us anomalous values on our early modulus measurements in which hand-drawn fibers were employed. However, both optical microscopy and electron microscopy quickly proved that these mechanically drawn fibers were indeed very nearly perfectly circular even in comparison with mechanically drawn wires such as tungsten, platinum, and piano wire. A typical electron micrograph of this series of examinations is shown in Figure 21. It will be noted that not only are these fibers circular but that they are structureless without any evidence of a second phase.

Table VI

Values for Young's Modulus on Mechanically Drawn Fibers of UARL Experimental Glasses
as Determined by Measurements on Tensile Test Equipment

Glass No.	Measured Modulus $\times 10^6$ psi	Standard Deviation Millions psi	Glass No.	Measured Modulus $\times 10^6$ psi	Standard Deviation Millions psi
25	12.3	1.9	131	12.5	
40	16.2	4.6	135	13.3	
56	10.7		136	13.5	
62	14.0		137	13.9	
63	13.0		138	12.2	
64	14.7		140	15.0	
65	13.8		155	14.7	1.9
66	14.6	2.0	157	13.1	2.8
67	12.7		159	15.7	5.0, 2.2
68	13.7		160	14.6	3.0
69	13.6		161	14.3	1.8
70	13.4		166	13.6	5.4
71	13.7		175	13.1	2.9
72	12.5		176	16.7	9.9
73	15.1		193	13.1	4.0
74	13.8		200	14.6	3.3
75	9.8		201	13.2	4.3
76	10.4		210	15.0	2.0
77	11.0		214	12.9	1.6
82*	13.3		215	13.3	3.0
83*	15.35	2.4, 1.95	235	15.3	1.9
97	10.4	1.7	237	18.8	7.9
98	10.8	2.5	238	15.2	3.2
102	13.3		260	10.4	1.5
108	12.5	2.7	261	11.5	1.8
110	13.8	2.2	275-0	27.6	17.8
114	15.1		275-I	14.9	6.3
126	16.15	1.82, 1.65	275-II	16.7	7.4
127	15.2		275-I	21.5	8.7
129	16.7	2.7, 2.6	275-II	19.7	6.8

Table VI (Contd.)

<u>Glass</u> <u>No.</u>	<u>Measured</u> <u>Modulus</u> <u>x 10⁶ psi</u>	<u>Standard</u> <u>Deviation</u> <u>Millions psi</u>	<u>Glass</u> <u>No.</u>	<u>Measured</u> <u>Modulus</u> <u>x 10⁶ psi</u>	<u>Standard</u> <u>Deviation</u> <u>Millions psi</u>
275-3-3	13.7, 14.2	1.8, 2.1	284	13.0	2.4
275-3-5	13.8, 14.0	3.0, 1.8	285	12.9	4.7
275-3-6	15.6, 16.5	2.7, 3.6	288-3	11.9	2.8
275-3-7	17.3, 16.2	7.2, 4.3	289	13.1	1.5
275-3-8	16.3, 16.4	3.8, 3.1	290-5	14.3	5.8
276	17.0	6.2	290-6	13.0	3.7
278	11.3	1.8	291	13.6	3.2
279	6.2	3.3	299	12.8	3.6
280	4.6	0.4	300	13.4	3.4
281	5.7	0.5	309	14.8	1.9
			E	11.8	3.9

All tabulated observations are the average of 20 observations except that the results for 40, 83, 126, 129 are averages of 60 observations and the result for 70 is the average of forty.

*82 - Houze Glass - U.S. 3,044,888

*83 - Owen-Corning - U.S. 3,122,277

Table VII

Correlation Between Standard Deviation in Young's Modulus
for Mechanically Drawn Fibers Measured on Tensile
Equipment and Standard Deviation in Diameter

<u>Glass Number</u>	<u>Measured Modulus (million psi)</u>	<u>Standard Deviation (millions psi)</u>	<u>Mean Diameter (mils)</u>	<u>Standard Deviation in Diameter (mils)</u>	<u>Minimum Diameter (mils)</u>	<u>Maximum Diameter (mils)</u>
201	13.2	4.3	2.71	0.62	1.41	3.74
210	15.0	2.0	1.33	0.32	0.89	1.87
214	12.9	1.6	1.20	0.23	1.01	2.12
215	13.3	3.0	1.38	0.09	1.20	1.56
235	15.3	1.9	1.37	0.23	1.01	1.81
237	18.8	7.9	1.25	0.25	0.64	1.63
238	15.4	3.2	1.61	0.43	0.92	2.39
276	17.0	6.2	1.48	0.39	0.89	2.35

The exceptionally high values for Young's modulus obtained for the glass fiber samples showing the large standard deviations in modulus measurements must, therefore, be considered an artifact. This artifact arises from the non-uniform diameter present in some of the experimental glasses and caused by crystalline inclusions. These inclusions are randomly scattered along the fiber and when present in sufficient quantity give rise to fictitious diameter measurements. No credence at this time can be placed in mechanical measurements made on fibers unless the fibers are free from defects causing bulges in the fiber which is fortunately true for most of the experimental glasses as may be seen from the standard deviations tabulated in Table VI.

The best solution to obtaining a meaningful measurement of the elastic modulus for those glasses where mechanical testing gave a large standard deviation would seem, therefore, to resort to methods independent of diameter measurements.

Young's Modulus for Mechanically Drawn Experimental Glass Fibers Evaluated By Ultrasonic Pulse Techniques

In our earlier report F910373-7 and F910373-8 we have given in detail our experiences in measuring Young's modulus using equipment manufactured by H. M. Morgan Co. Inc., Cambridge, Mass. These experiments carried out at several locations (Fabric Research Laboratories, H. M. Morgan Co. & UARL) using several models of the Morgan Dynamic Modulus Tester RPM-5R did not yield data consistent with either UARL sonic measurements on bulk samples or mechanical measurements on mechanically drawn glass fibers. This approach was, therefore, discarded even though it possessed the marked advantage of not requiring a diameter measurement.

At this time, therefore, a different approach to sonic modulus measurements on glass fibers was taken. This method in contrast to the Morgan Co. method is not a resonance technique but uses a measurement of the transit time of ultrasonic pulse and requires only a time measurement, a length measurement, and a density measurement. The measurements were made for us by Panametrics, Inc. of Waltham, Mass. using a modification of their ultrasonic thermometer, the Pana-therm Model 5000. Using selected specimens as free as possible from bulges due to inclusions, measurements were made on UARL 275 glass fibers with the following results.

Ultrasonic Pulse Modulus Measurements - Glass 275

<u>Specimen Number</u>	<u>Young's Modulus (Millions psi)</u>
1	15.77, 15.96, 15.50, 16.27
3	15.67, 15.77
5	15.98, 16.33
7a	16.00, 16.09
7b	15.91, 16.11
9	15.95, 16.19
11	15.77, 16.12

It is apparent, therefore, that the correct modulus for this glass is approximately 16.0 million psi instead of the 20.0 million psi obtained by averaging the first hundred mechanical measurements on these glass fibers.

Selected fiber specimens were also sent to Lowell Institute of Technology for check modulus evaluations by mechanical testing but this work is not yet complete.

Purchase of Single Hole Platinum Bushings for
Improving Fiberization Processes

The work described in the two previous sections made it obvious, that just as for accurate strength determinations so for some glasses for accurate modulus measurements, a defect-free fiber is essential.

In the future this method of drawing fibers will be supplemented through the use of a single-hole glass bushing of the more conventional type as shown in Fig. 24. This design is a UARL design combining hopefully the best features of single-hole bushings described by Tiede (Ref. 32) and the National Bureau of Standards (Ref. 33). Two bushings of this design are scheduled for delivery in late December with installation in January.

CONCLUSIONS

1. This contract to-date, has produced three promising directions in which to move in search of high-modulus high-strength glass fibers.

- a. The cordierite glass system with rare earths and/or zirconia as major constituents has yielded bulk glass specimens with values for Young's modulus as high as 19.23 million psi.

- b. The UARL development of invert analog glass systems has produced bulk glass specimens with values for Young's modulus of 20.7 million psi and specific moduli in hybrid units of 6.82 to 7 million psi per gram per cubic centimeter.
- c. A preliminary exploration of two phase glass systems has indicated that the second phase develops so rapidly that it can be produced as the glass fiber is drawn with subsequent pronounced improvement in modulus.

2. The UARL invert analog glass systems include six to fifteen components so that it is likely that finding the optimum modulus in such systems will require mathematical analysis to relate choice of composition to modulus, density, liquidus, and working range. More data of this type is needed to improve the application of a computer program.

3. The making of glass fiber sufficiently free of defects to provide consistent strength measurements required a conventional type single-hole glass bushing. Such a bushing will be incorporated in the program in the next quarter.

4. For glass fibers of non-constant diameter due to occasional crystalline inclusions the ultrasonic pulse technique of modulus measurement is capable of yielding consistent data.

PERSONNEL ACTIVE ON PROGRAM

Personnel active on the program throughout the eleventh, twelfth, and thirteenth quarters have been, James F. Bacon, Principal Investigator. Throughout the eleventh quarter and most of the twelfth quarter Norman S. Chamberlain, Senior Experimental Technician was intimately connected with the program. In the final month of the twelfth quarter and the first two months of the thirteenth quarter, Robert B. Graf, rejoined the program and resumed the optical studies of crystallization kinetics. The electron microprobe analysis was carried out for us by Archie Manzione. Liaison throughout the program has been furnished by Peter A. Stranges of the UARL Washington Office. Throughout the program the UARL personnel have reported progress to and received advice from James Gangler of NASA Washington Headquarters and Michael DeCrescente of UARL. At the end of the twelfth quarter Michael DiPerno and Francis Hale joined the program as experimental technicians and have continued throughout the thirteenth quarter.

Various services have been carried out for us in connection with the program by the metallography, electron microscopy, and chemical analysis groups of UARL, by the Glass Testing Laboratory of Emhart Corporation, by the Textile Research Foundation of Lowell Institute of Technology, and by Panametrics, Inc. of Waltham, Massachusetts. To all concerned we say thanks.

REFERENCES

1. Klingsberg, C. (Editor): The Physics and Chemistry of Ceramics. Gilman, J. J.: The Strength of Ceramic Crystals. Gordon & Breach, New York, 1963, pp 246-274.
2. Wells, A. F.: Structural Inorganic Chemistry, 3rd ed., Oxford Univ. Press, London, 1962.
3. Weyl, W. A. and Marboe, E. C.: The Constitution of Glasses, Vol. II: Constitution and Properties of Some Representative Glasses, Part I. Interscience Publishers (John Wiley & Sons), New York, pp 757-790 and Section 5, p 531, 1964.
4. Rawson, H.: Inorganic Glass-Forming Systems, Academic Press, London and New York, (1967).
5. Stanworth, J. E.: Physical Properties of Glass, Oxford Univ. Press, London (1950).
6. Tiede, R. L., U.S. 3,127,277; U.S. 2,640,784; U.S. 2,571,074; U.S. 3,132,033; U.S. 2,640,784.
7. Armistead, W. H., U.S. 2,517,459 and U.S. 2,433,883.
8. Bastian, R. R. and A. C. Ottojon, U.S. 2,978,341.
9. Labino, D., U.S. 2,685,526.
10. Ram, Atma, S. N. Prasad, and K. P. Srivastava: Viscosity of Copper Ruby Glass in and Below the Striking Range of Temperature, Glass Technology, Vol. 9, No. 1, p 1-4, Feb. 1968.
11. Weyl, W. A. and E. C. Marboe: The Constitution of Glasses, Volume I. Interscience Publishers (a division of John Wiley & Sons), New York, pp. 245-248, 1962.
12. Krebs, H.: The Structure of Glasses. Angew. Chem., International Edition, Vol. 5 (1966), No. 6, pp. 544-554.
13. Argyle, J. F. and F. A. Hummel: Liquid Immiscibility in the System BaO-SiO₂. Physics and Chem. of Glasses 4, 103-105, 1963.

REFERENCES (Contd.)

14. Cahn, J. W. and R. J. Charles: The Initial Stages of Phase Separation in Glasses. Physics and Chem. of Glasses 6, 5, 181-191, October 1965.
15. Charles, R. J.: Phase Separation in Borosilicate Glasses. Journ. Am. Cer. Soc., Vol. 47, No. 11, pp. 559-563, November 1964.
16. Herczog, A.: Microcrystalline BaTiO_3 by Crystallization from Glass. Journ. Am. Cer. Soc. 47, 107-115.
17. Hummel, F. A., T. Y. Tien and K. H. Kim: Studies in Lithium Oxide Systems: VIII, Application of Silicate Liquid Immiscibility to Development of Opaque Glazes. Journ. Amer. Cer. Soc., Vol. 43, No. 4, pp. 192-197, April 1960.
18. Johnson, D. W. and F. A. Hummel: Phase Equilibria and Liquid Immiscibility in the System $\text{PbO-B}_2\text{O}_3\text{-SiO}_2$. J. Amer. Cer. Soc., Vol. 31, 4, 196-201, April 1968.
19. Levin, E. M. and G. W. Cleek: Shape of Liquid Immiscibility Volume in the System Barium Oxide-Boric Oxide-Silica. J. Amer. Cer. Soc., Vol. 41, No. 5, pp. 175-179, May 1958.
20. Ohlberg, S. M., H. R. Golob, C. M. Hollabaugh: Fractography of Glasses Evidencing Liquid-in-Liquid Colloidal Immiscibility. J. Am. Cer. Soc., Vol. 45, No. 1, 1-4, January 1962.
21. Ohlberg, S. M., J. J. Hammel and H. R. Golob: Phenomenology of Non-Crystalline Microphase Separation in Glass. J. Am. Cer. Soc., Vol. 48, No. 4, pp. 178-180, April 1965.
22. Rindone, G. E.: Further Studies of the Crystallization of a Lithium Silicate Glass. Jour. Am. Cer. Soc., Vol. 45, 1, 7-12, January 1962.
23. Rockett, T. J., W. R. Foster and R. G. Ferguson, Jr.: Metastable Liquid Immiscibility in the System Silica-Sodium Tetraborate. J. Am. Cer. Soc. 48, 6, 329-332, June 1965.
24. Roy, R.: Metastable Liquid Immiscibility and Nucleation Subsolidus. J. Am. Cer. Soc. 43, 670-671.
25. Sastry, B. S. R. and F. A. Hummel: Studies in Lithium Oxide Systems: III, Liquid Immiscibility in the System $\text{Li}_2\text{O-B}_2\text{O}_3\text{-SiO}_2$. J. Am. Cer. Soc. Vol. 42, 2, pp. 81-88, February 1959.

REFERENCES (Contd.)

26. Tichane, R. M. and G. B. Carrier: Microstructure of a Soda-Lime Glass Surface. J. Am. Cer. Soc., Vol. 44, No. 12, pp. 606-610, December 1961.
27. Tran, T. L.: Study of Phase Separation and Devitrification Products in Glasses of the Binary System, $\text{Na}_2\text{O}-\text{SiO}_2$.
28. Watanabe, M., H. Noake and T. Aiba: Electron Micrographs of Some Borosilicate Glasses and Their Internal Structure. J. Am. Cer. Soc., Vol. 42, No. 12, pp. 593-599.
29. Janakiramaraao, Bh. V.: Neo-Ceramic Glasses and Their Structure. Glass Technology, Vol. 5, No. 2, 67-77, April 1964.
30. Morley, J. G.: Crystallization Kinetics In Some Silicate Glasses, Part I. Apparatus for the Direct Measurement of Crystal Growth at High Temperatures, Glass Technology, Vol. 6, No. 3, pp 69-76.
31. Tiede, R. L.: Improved Apparatus for Rapid Measurement of Viscosity of Glass at High Temperature. J. Amer. Ceramic Soc., Vol. 42, 1959, pp. 537-541.
32. Tiede, R. L.: Viscometer for Measuring Glass Viscosity by Means of Flow Through An Orifice, J. Amer. Cer. Soc., Vol. 38, No. 5, pp. 183-186, May 1955.
33. Capps, Webster & Douglas H. Blackburn, N.B.S. No. 5188, The Development of Glass Fibers Having Young's Moduli of Elasticity, Nat. Bur. Standards, April, 1957.

STRUCTURE IN GLASS



STRUCTURE IN GLASS



278a @ 800°C

20,000X

STRUCTURE IN GLASS



278b @ 800°C

20,000X

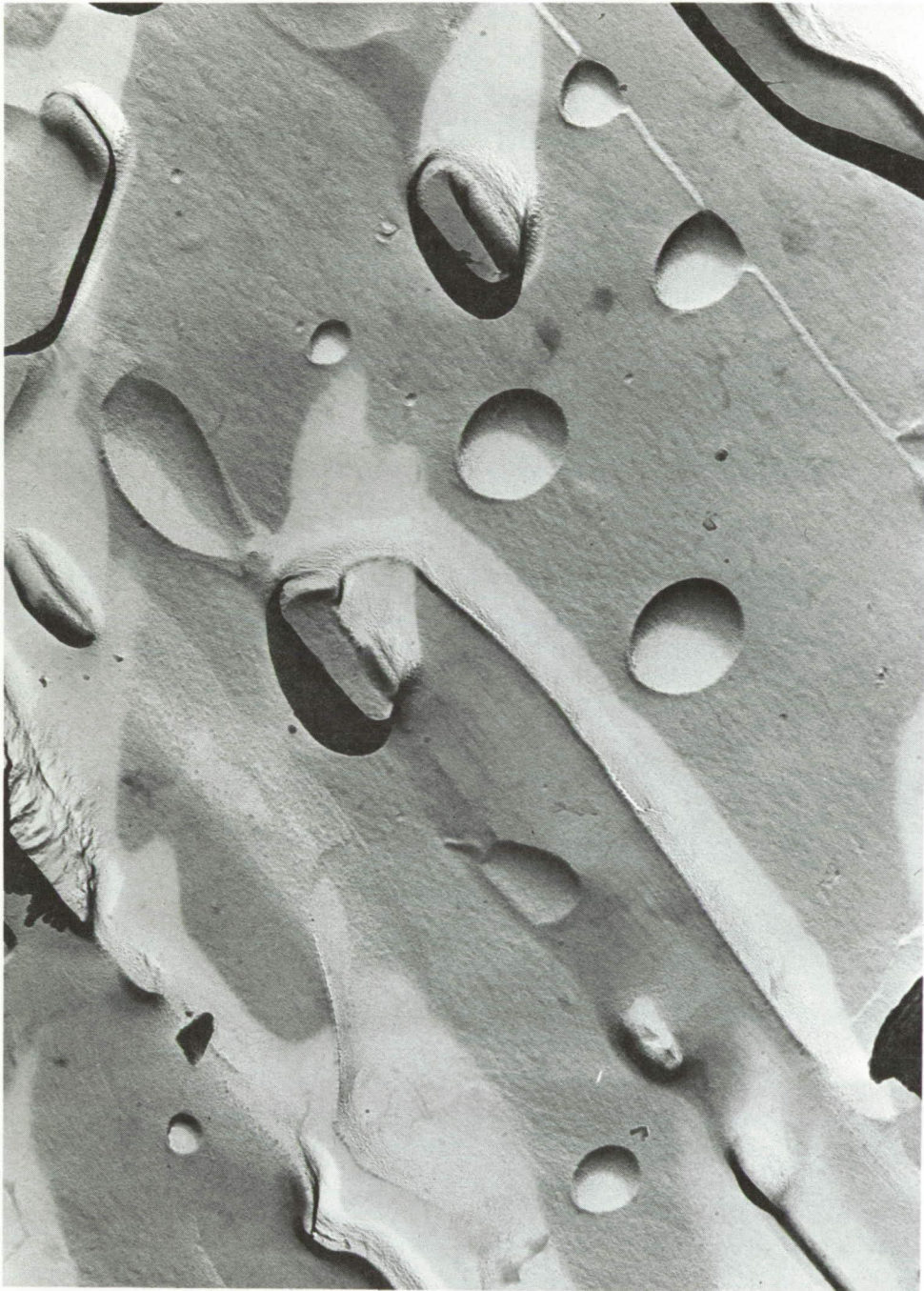
STRUCTURE IN GLASS



279a

30,000X

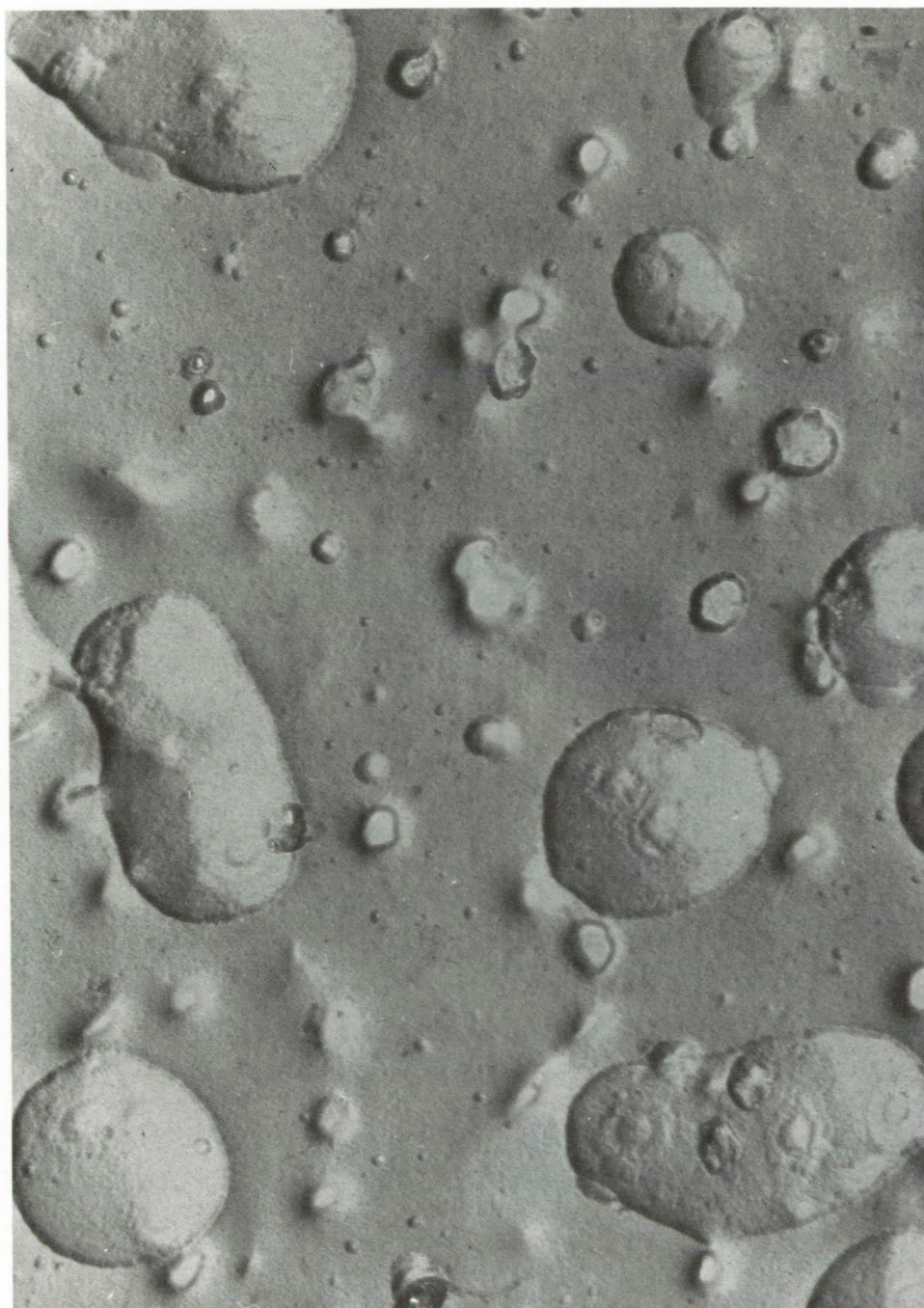
STRUCTURE IN GLASS



279a @ 900°C

20,000X

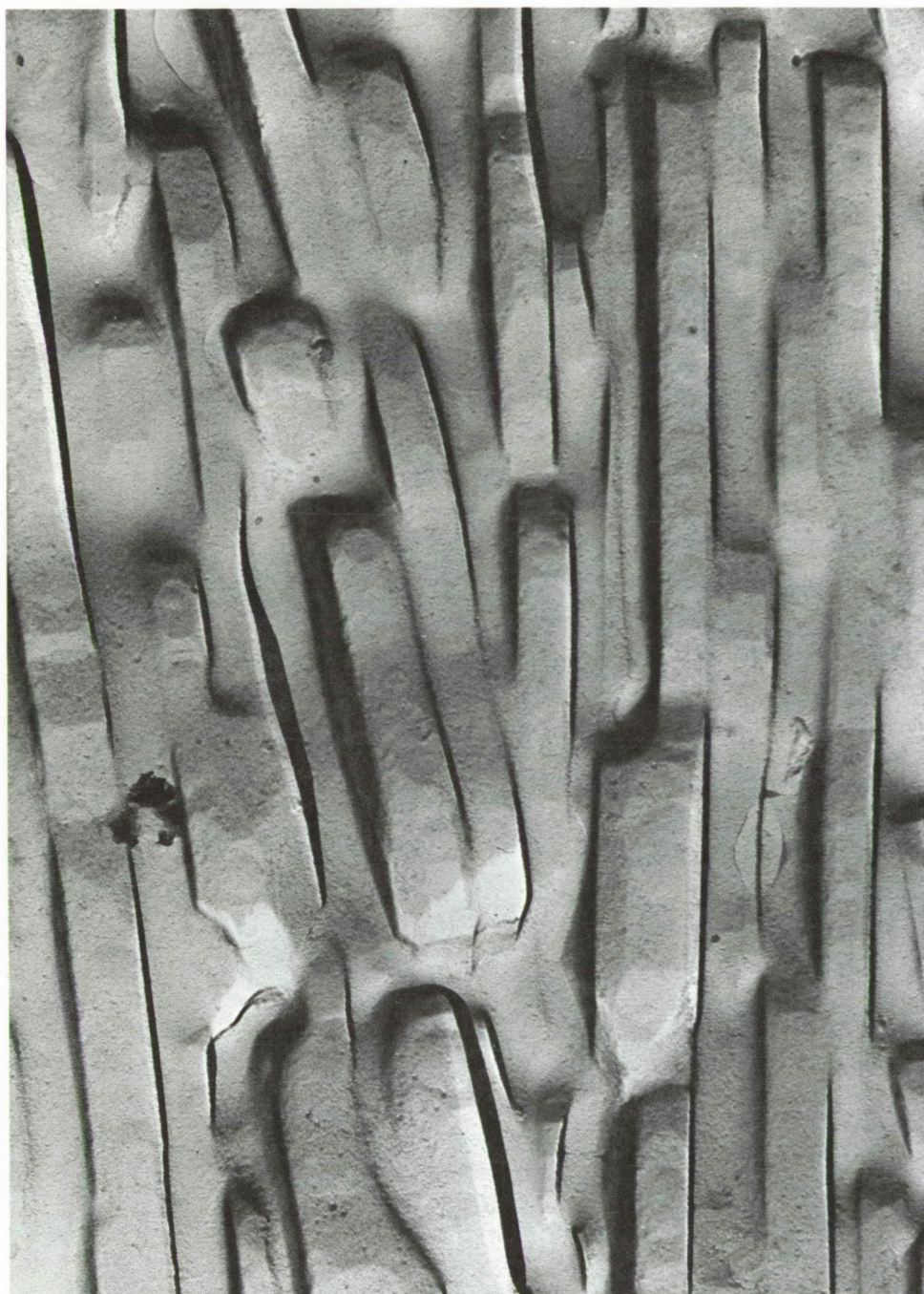
STRUCTURE IN GLASS



279bi @ 900° C

20,000X

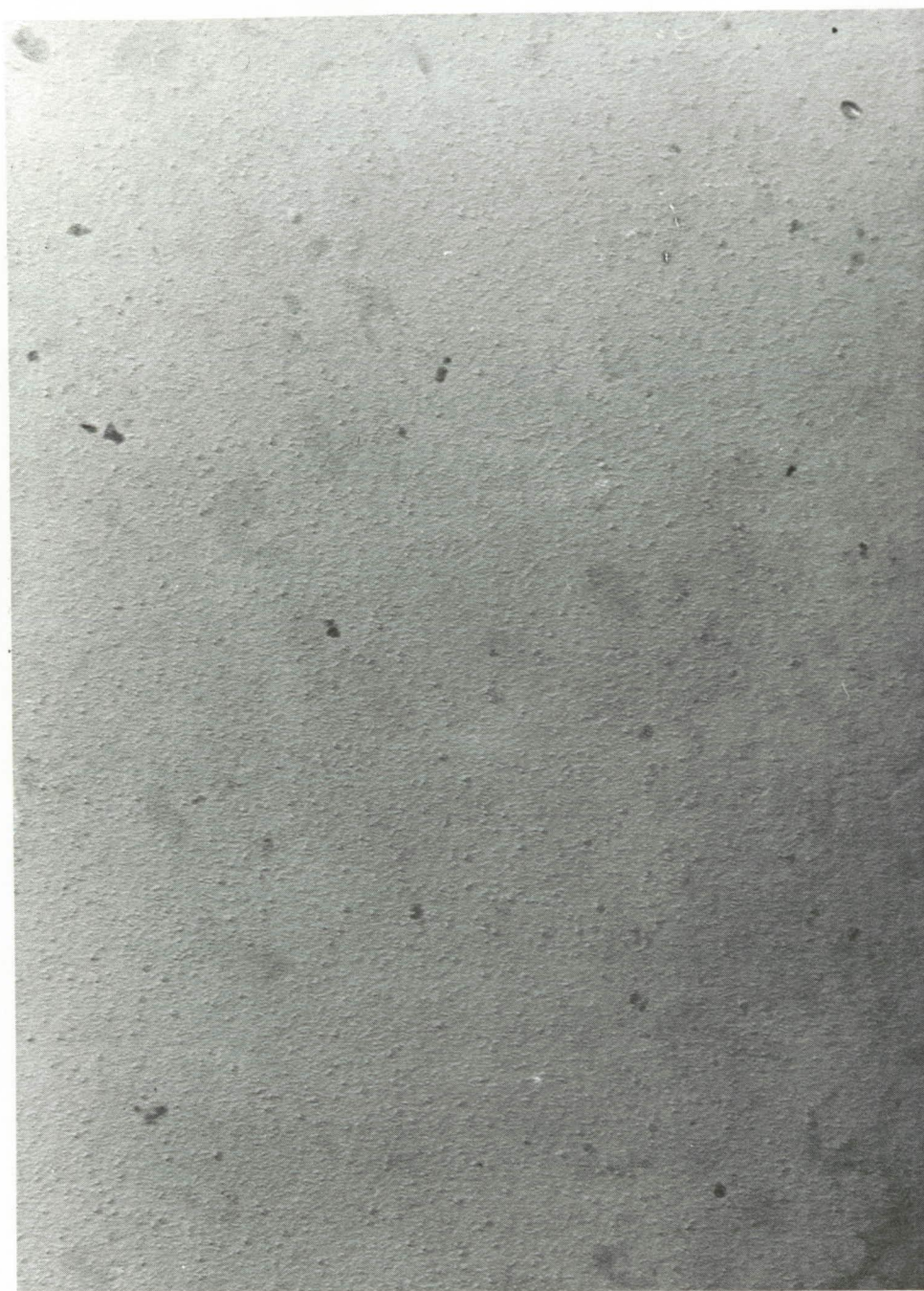
STRUCTURE IN GLASS



279bo @ 900°C

20,000X

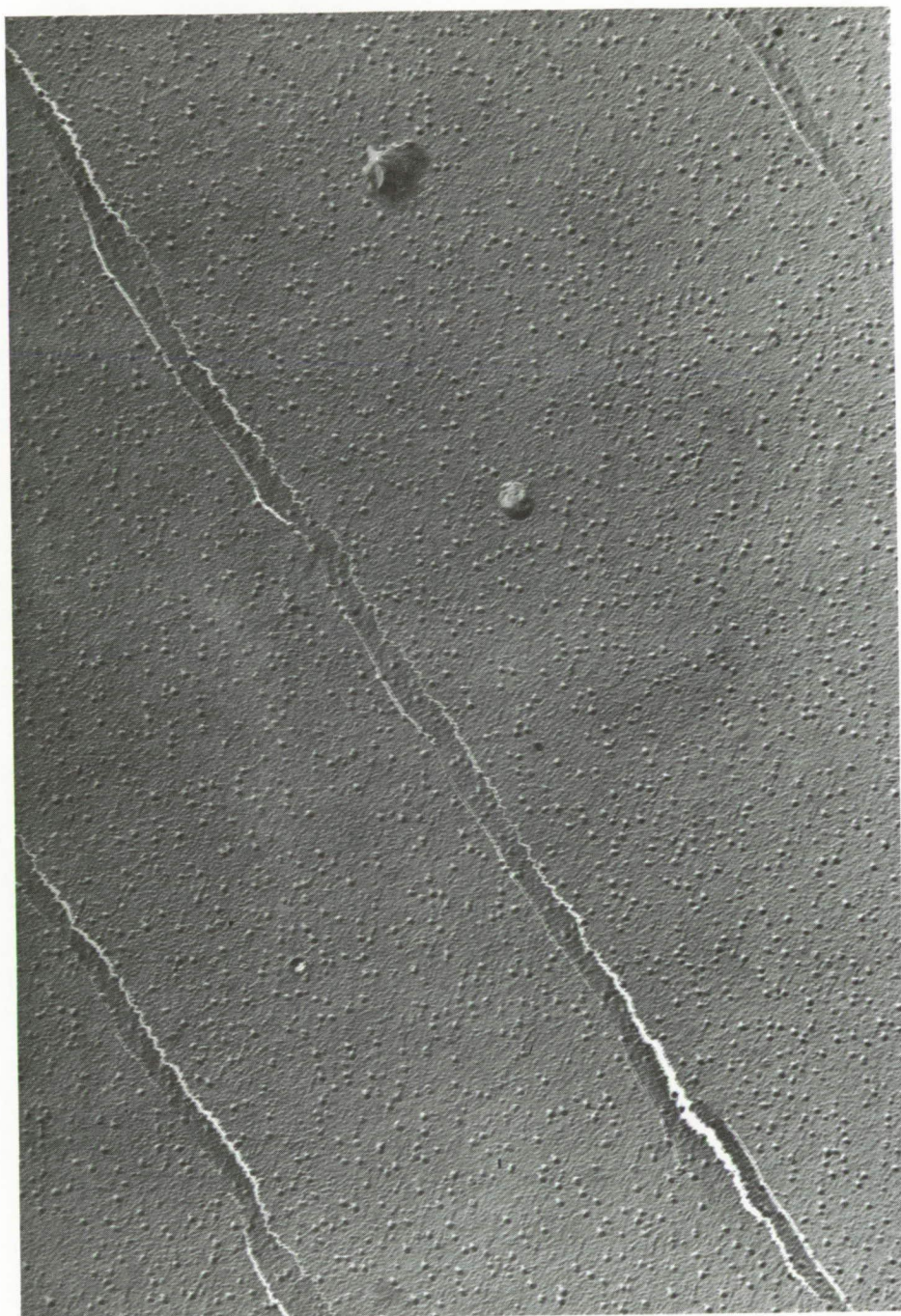
STRUCTURE IN GLASS



280a

30,000X

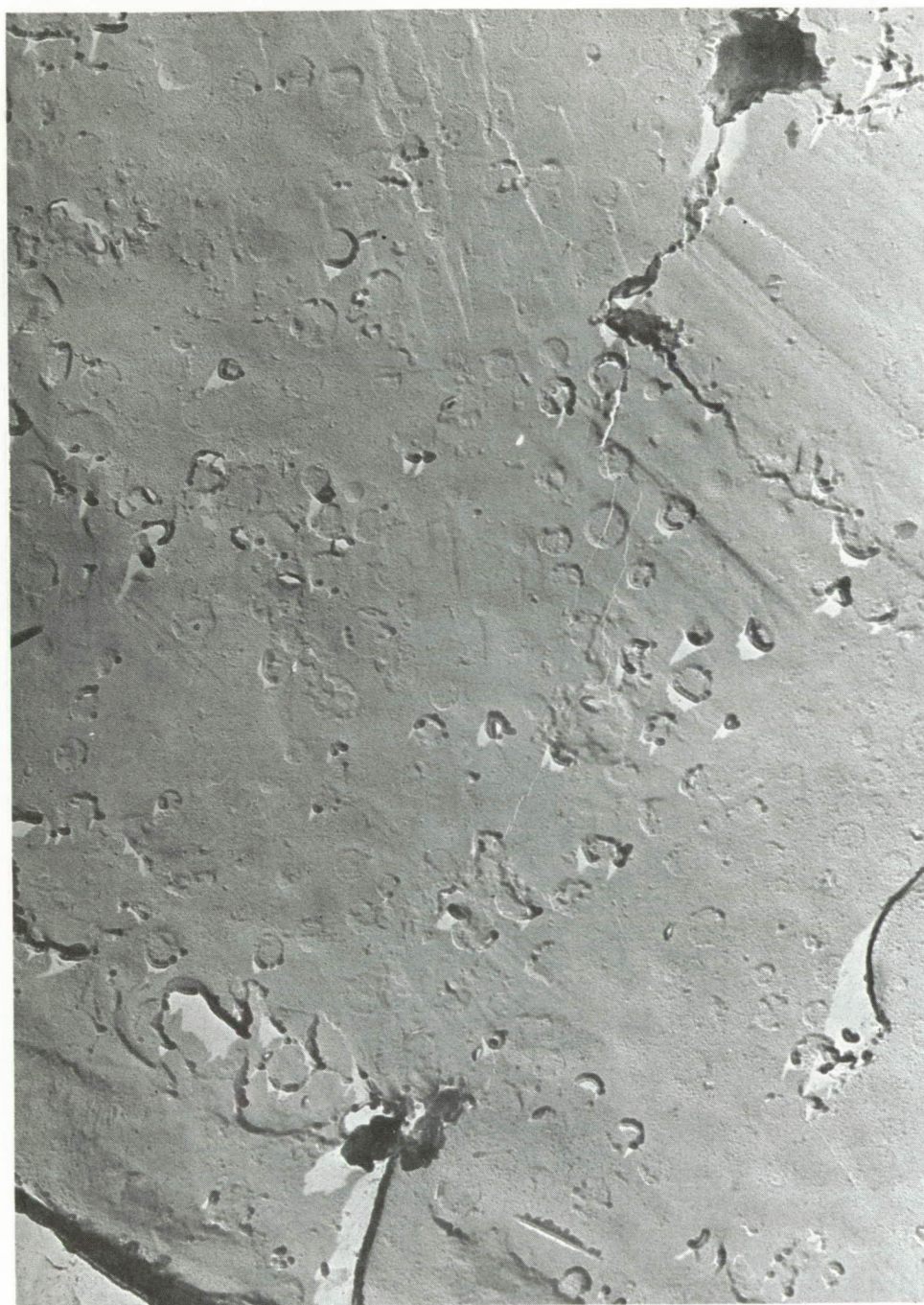
STRUCTURE IN GLASS



280 @ 650°C

20,000X

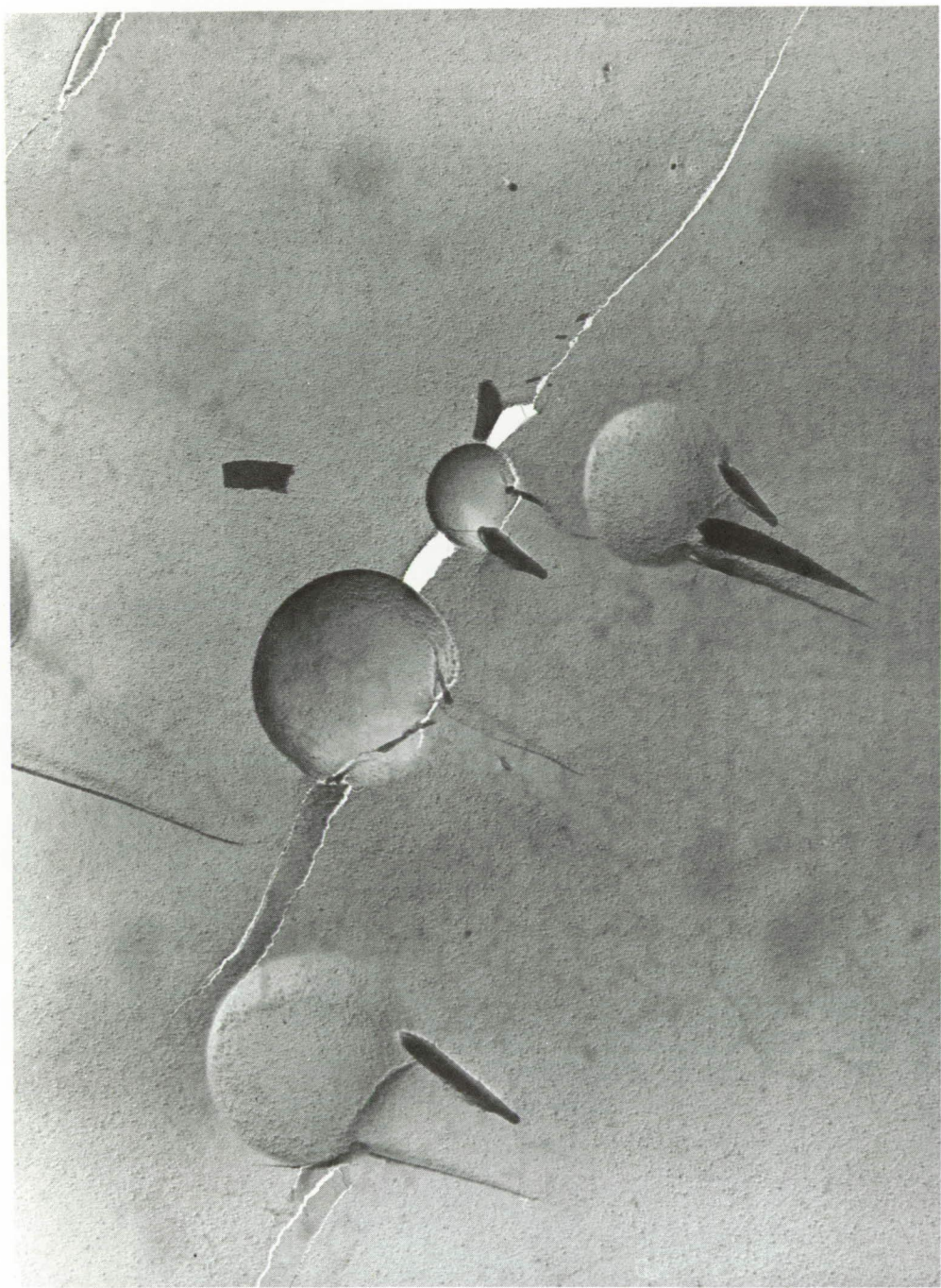
STRUCTURE IN GLASS



281

20,000X

STRUCTURE IN GLASS



281b @ 900°C

20,000X

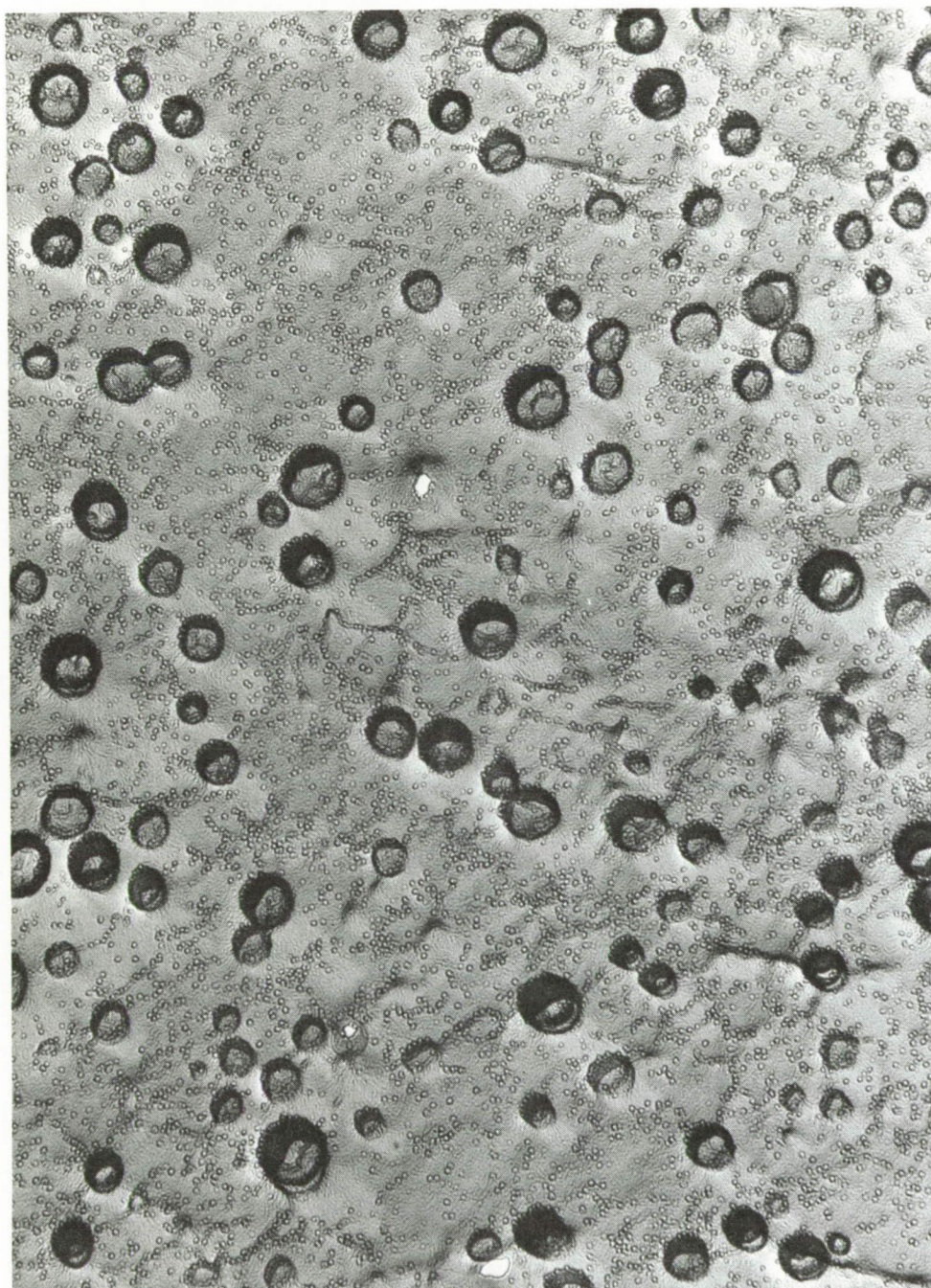
STRUCTURE IN GLASS



STRUCTURE IN GLASS



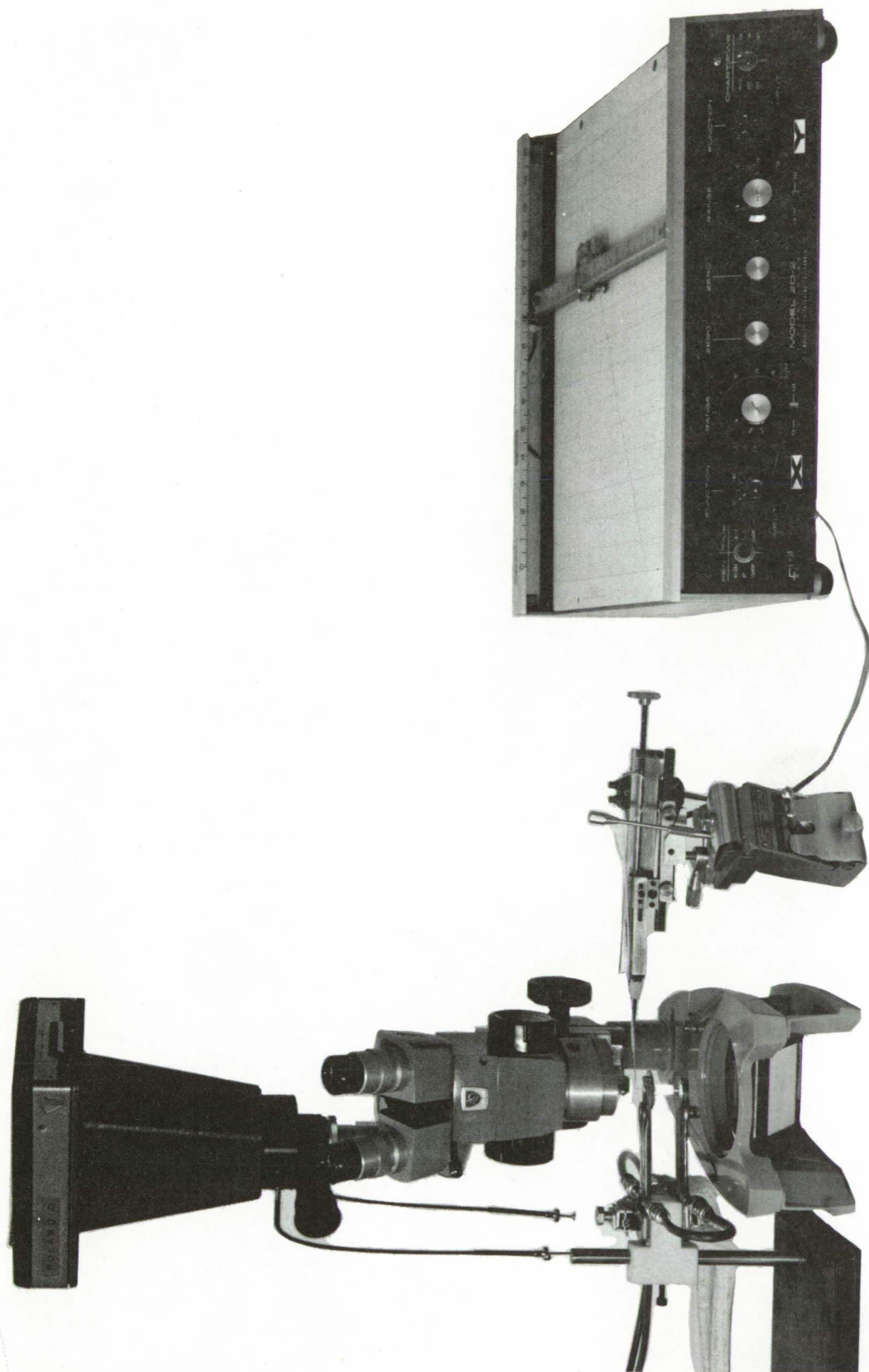
STRUCTURE IN GLASS



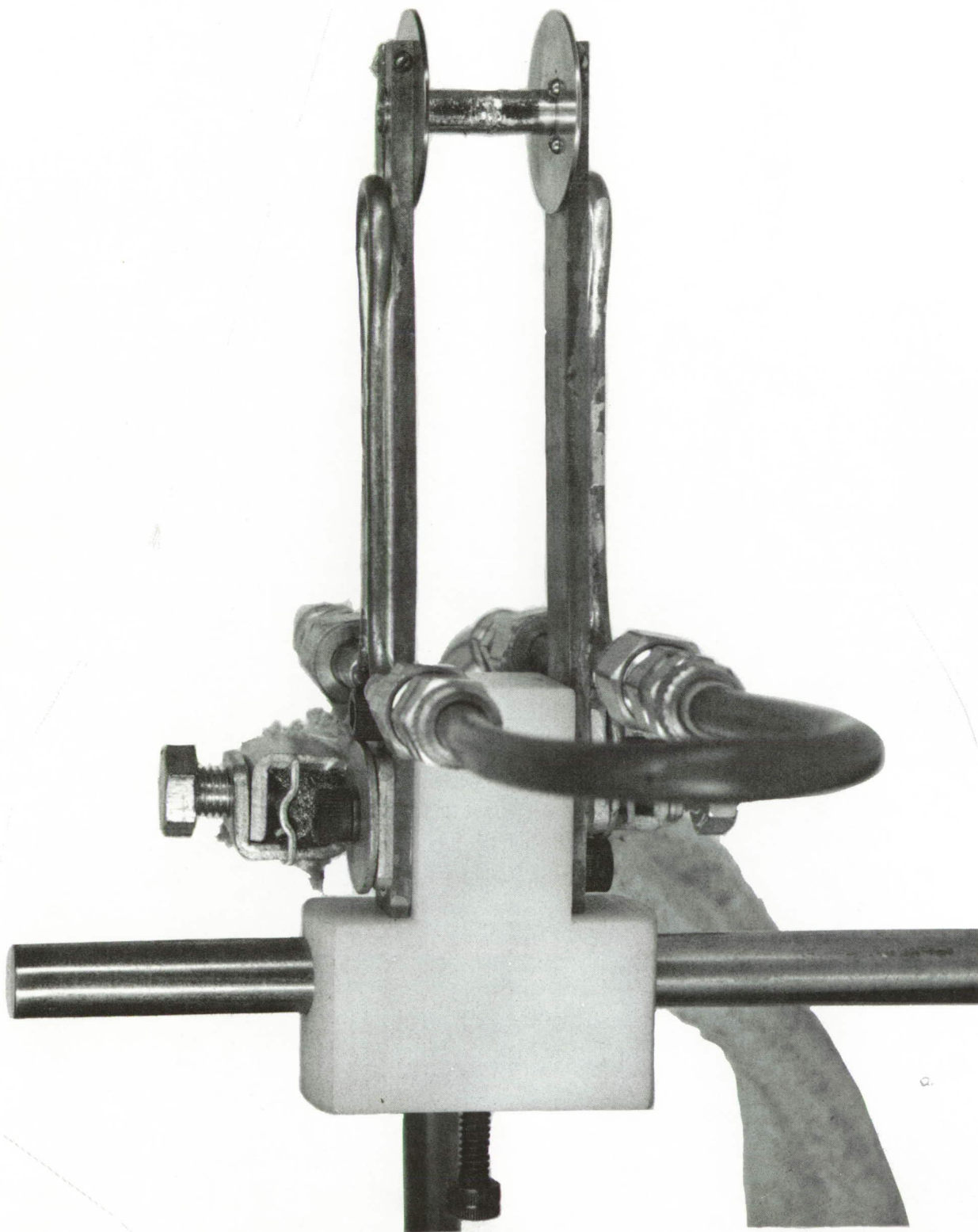
282a @ 650°C

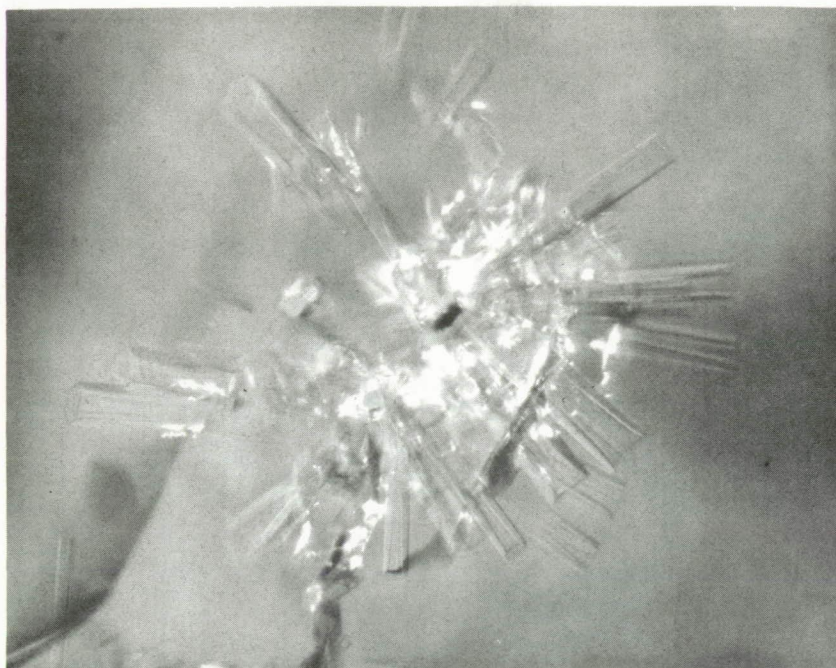
20,000X

CLOSE-UP OF MICRO-FURNACE, HEAT SHIELDS REMOVED



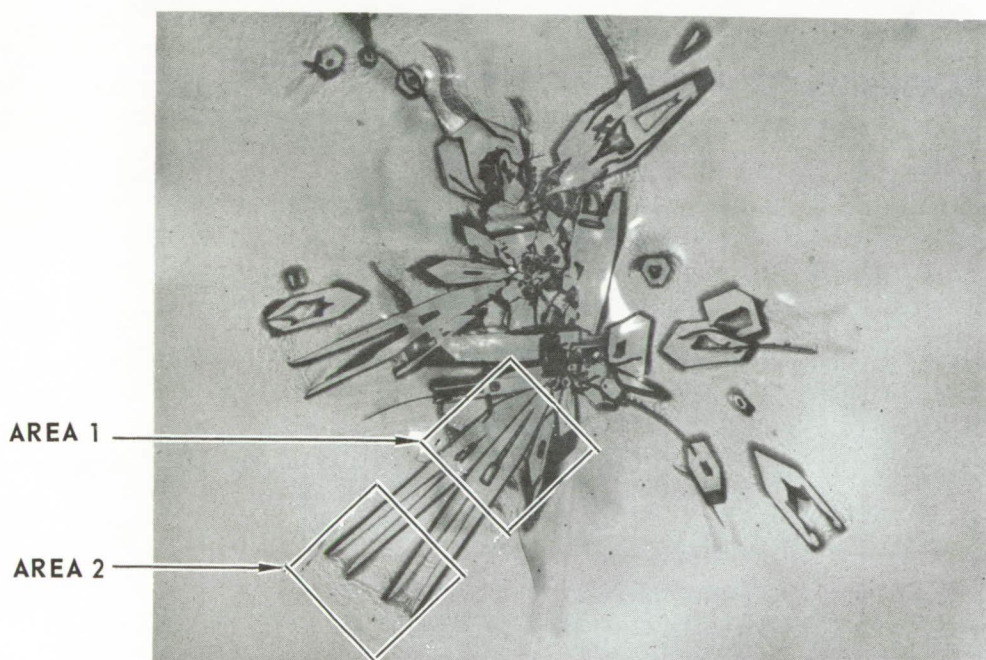
MICRO-FURNACE IN POSITION FOR USE





17 A TRANSMITTED LIGHT

100X

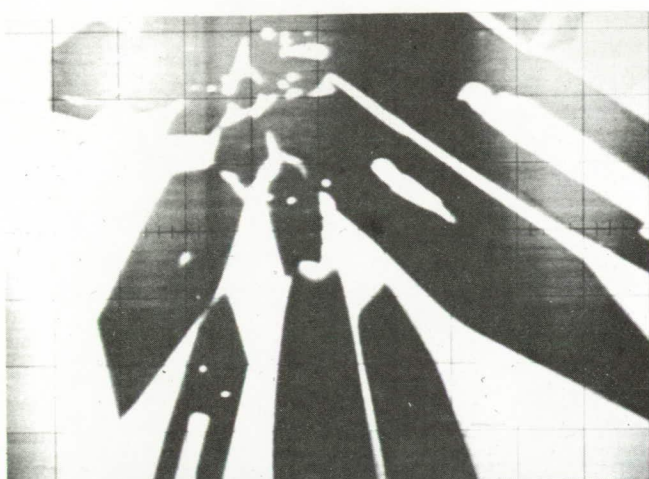


17 B REFLECTED LIGHT

ETCHED CONDITION

100X

LIGHT PHOTOMICROGRAPHS SHOWING THE APPROXIMATE LOCATIONS OF BEAM
SCAN ANALYSES.



SPECIMEN CURRENT

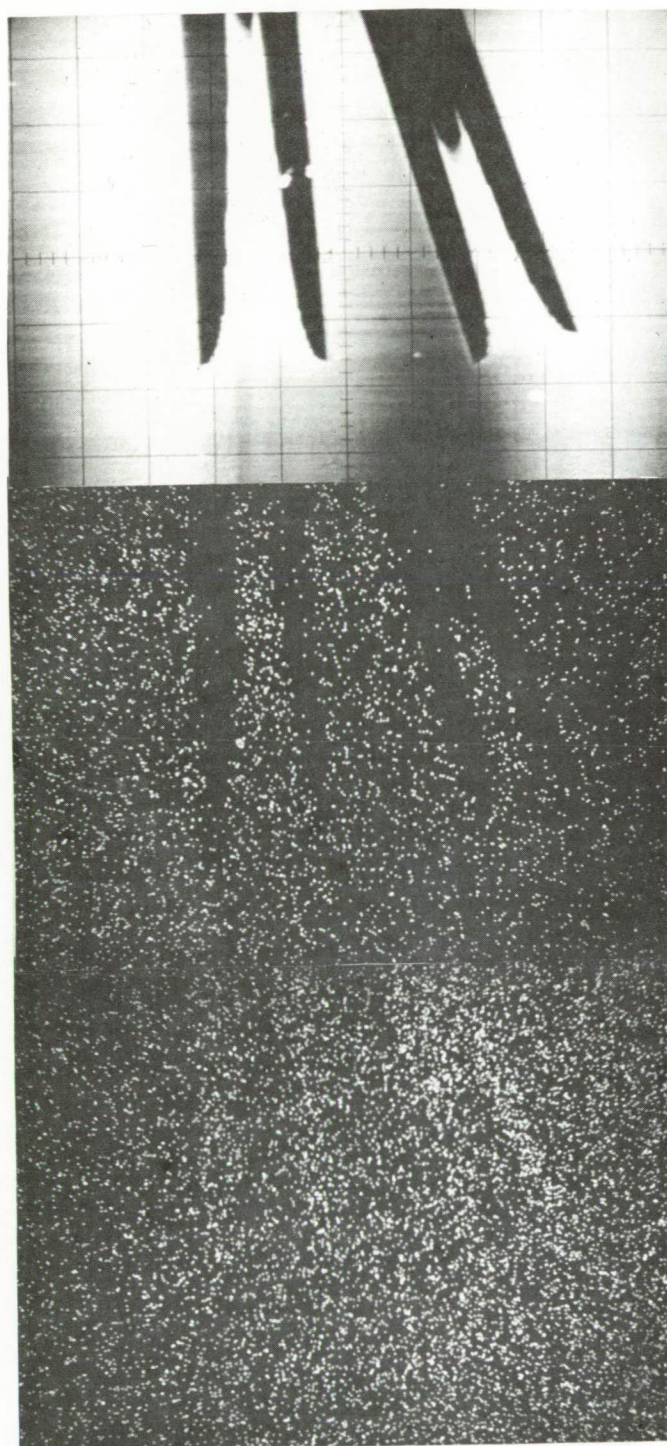


LANTHANUM X-RAYS

ALUMINUM X-RAYS

MAG: 330X

ELECTRON BEAM SCAN ANALYSIS OF AREA 1 AS INDICATED IN FIG. 1 B.
THE CRYSTALS APPEAR DARKER INDICATING THEM TO BE OF LOWER ATOMIC
NUMBER THAN THE MATRIX.



SPECIMEN CURRENT

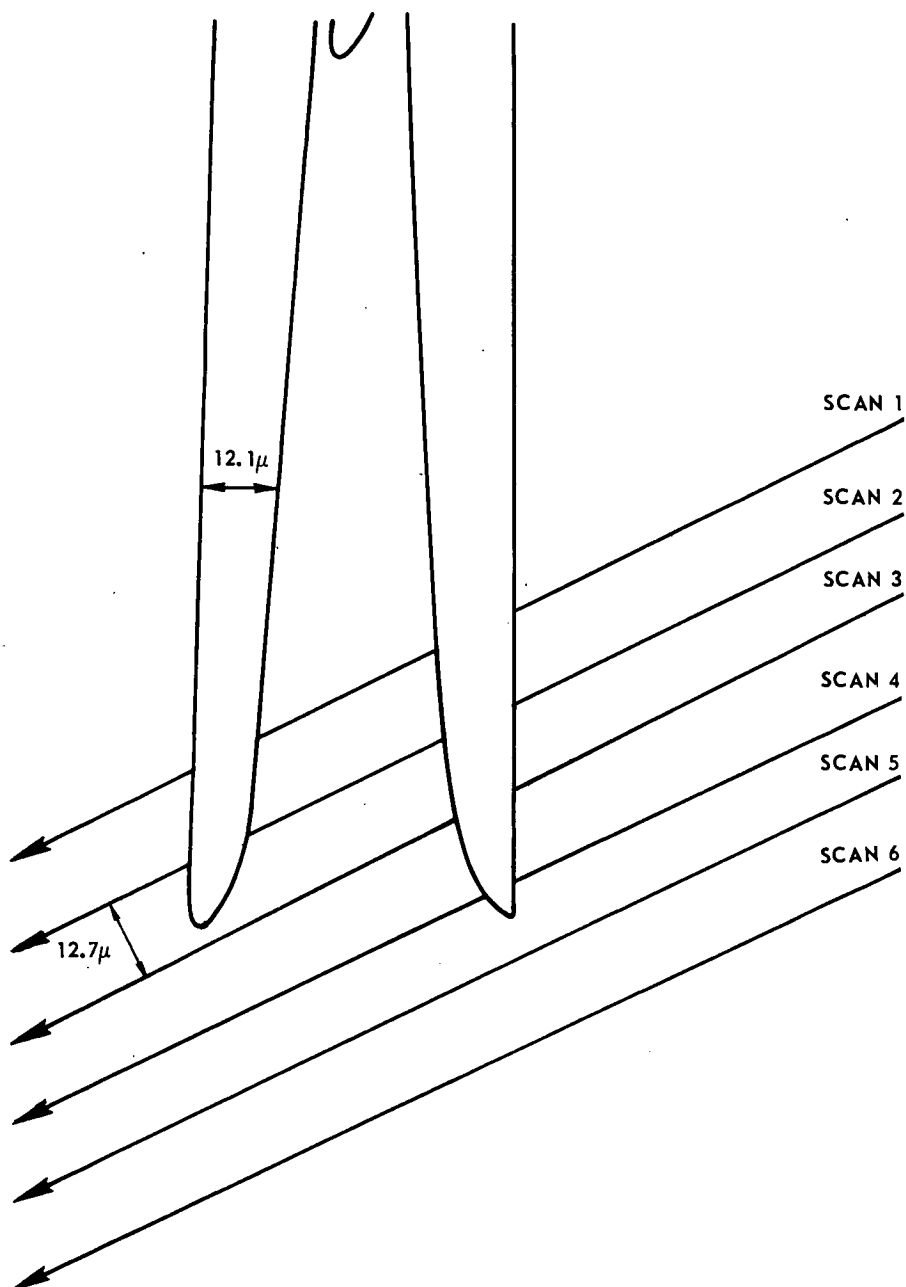
LANTHANUM X-RAYS

ALUMINUM X-RAYS

MAG: 330X

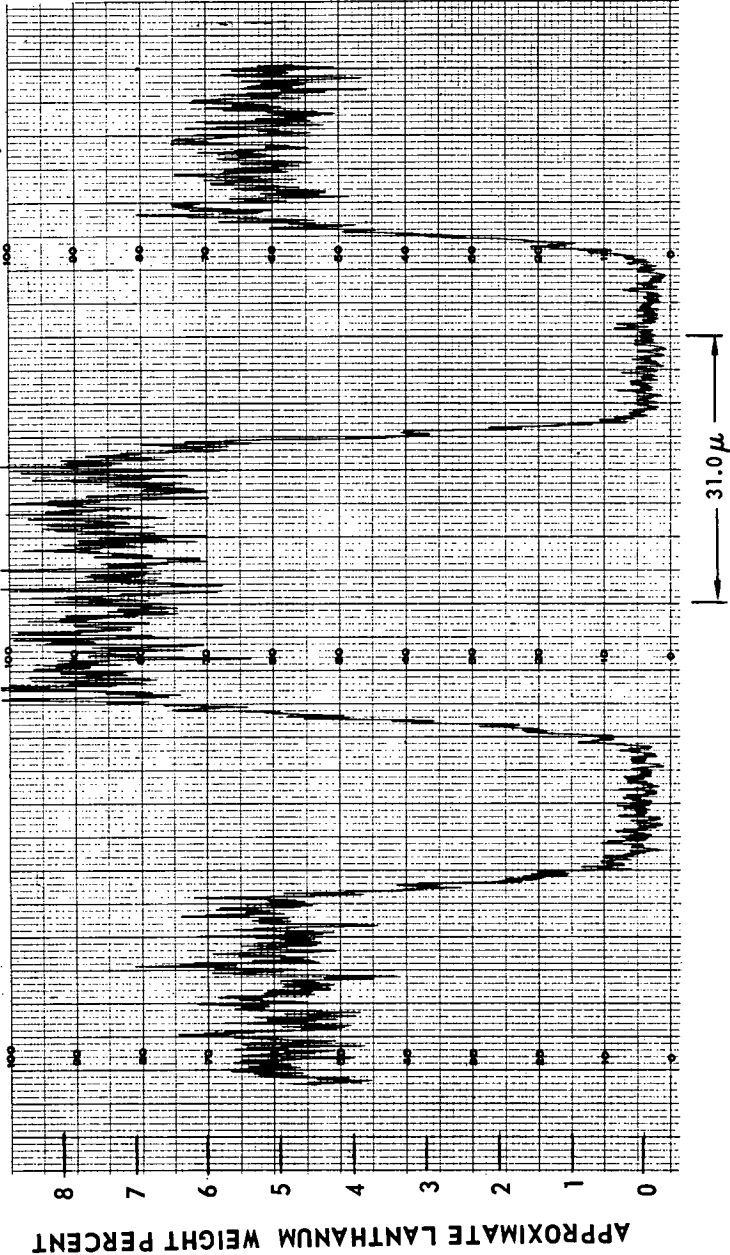
ELECTRON BEAM SCAN ANALYSIS OF AREA 2 AS INDICATED IN FIG. 1B.
THE LANTHANUM DISTRIBUTION SCANS WERE ALSO OBTAINED IN THIS
AREA (REF FIG. 3).

THE LANTHANUM DISTRIBUTIONS ACROSS THESE PATHS ARE GIVEN IN FIGS. 4a-4f



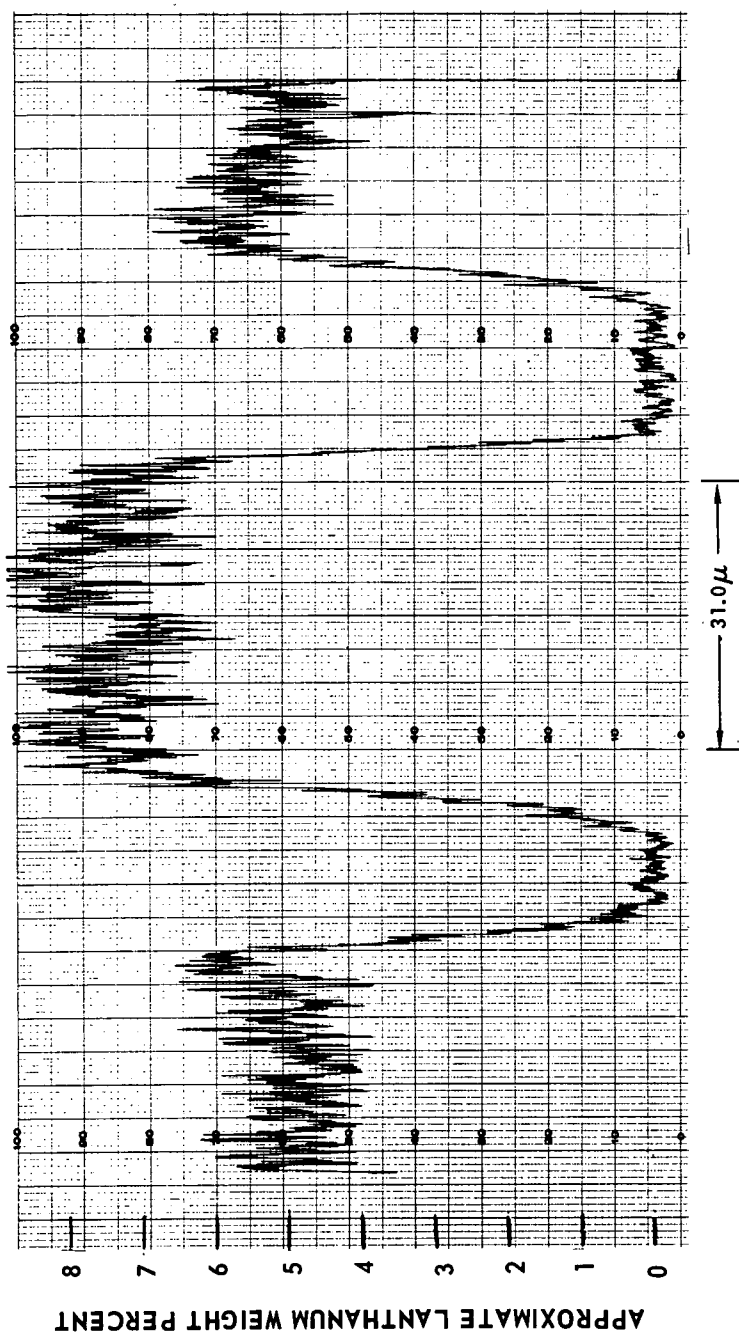
SCHEMATIC REPRESENTATION OF THE PATHS SCANNED BY THE
ELECTRON BEAM

SCAN 1



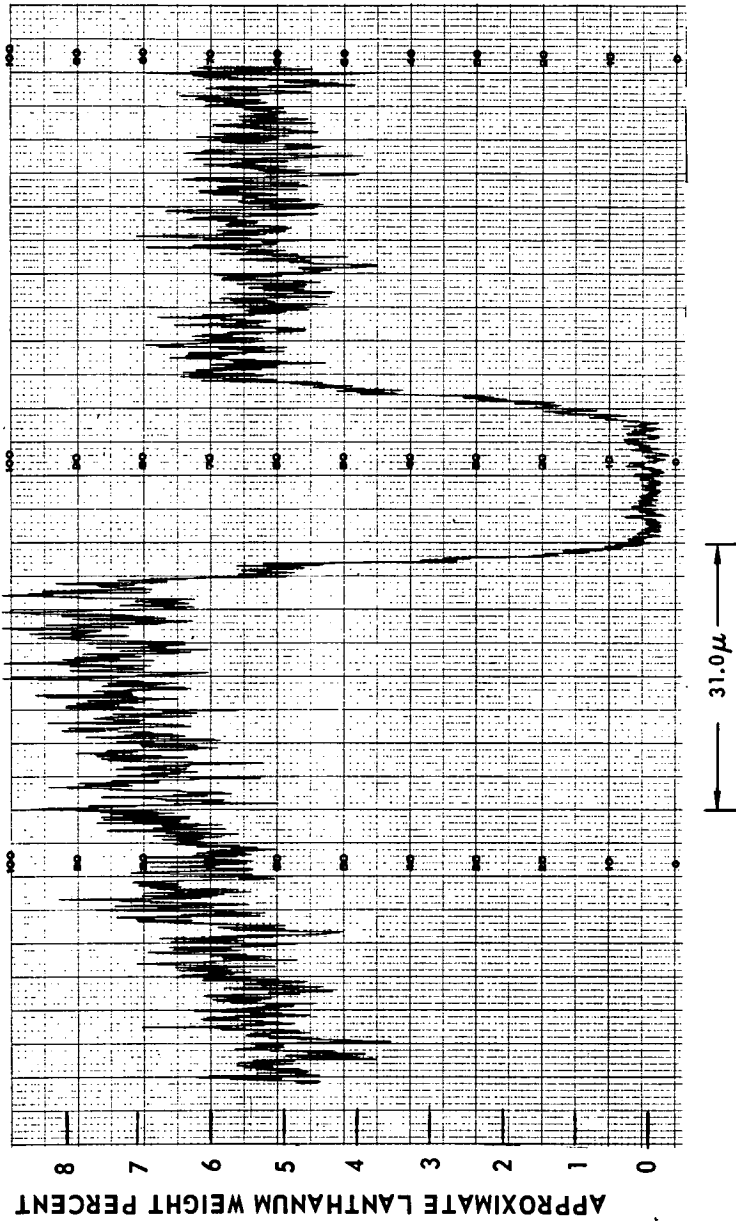
LANTHANUM DISTRIBUTION SCANS ACROSS PATH SHOWN SCHEMATICALLY IN FIG. 19

SCAN 2

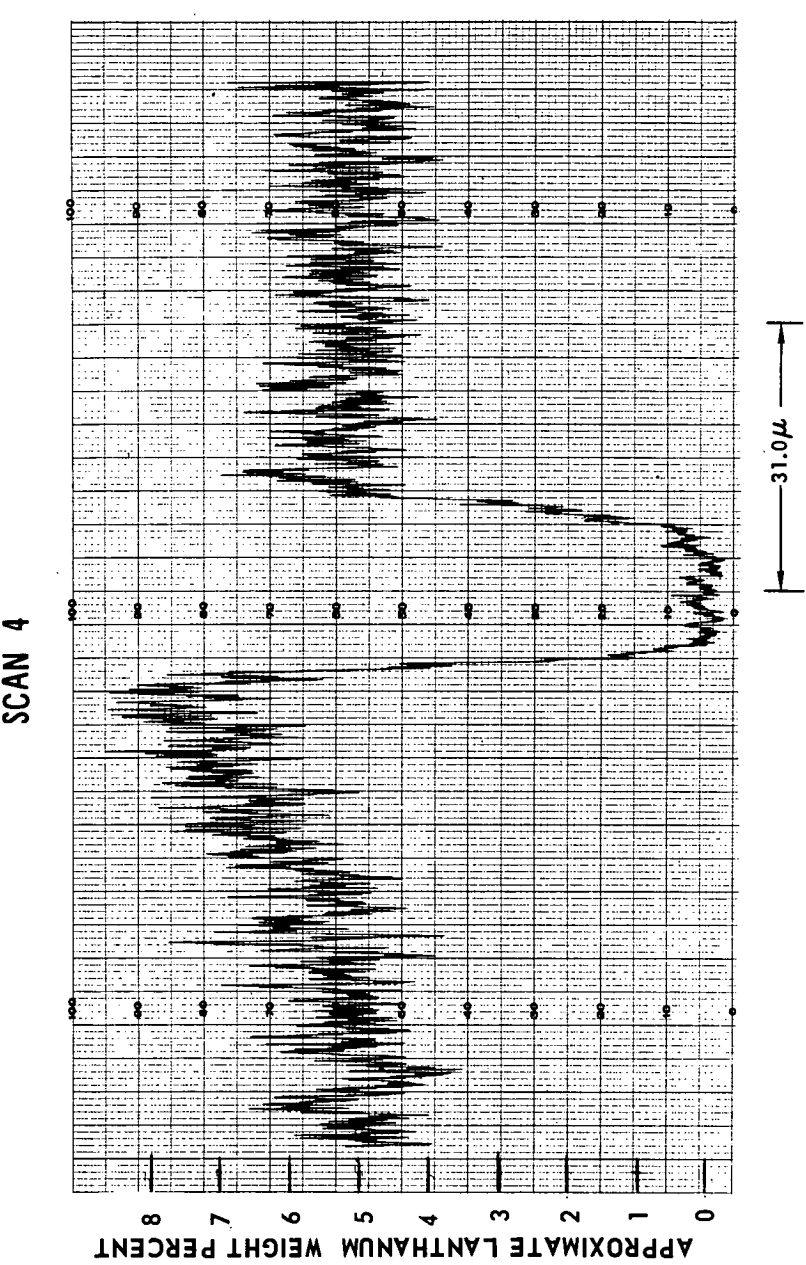


LANTHANUM DISTRIBUTION SCANS ACROSS PATH SHOWN SCHEMATICALLY IN FIG. 19

SCAN 3

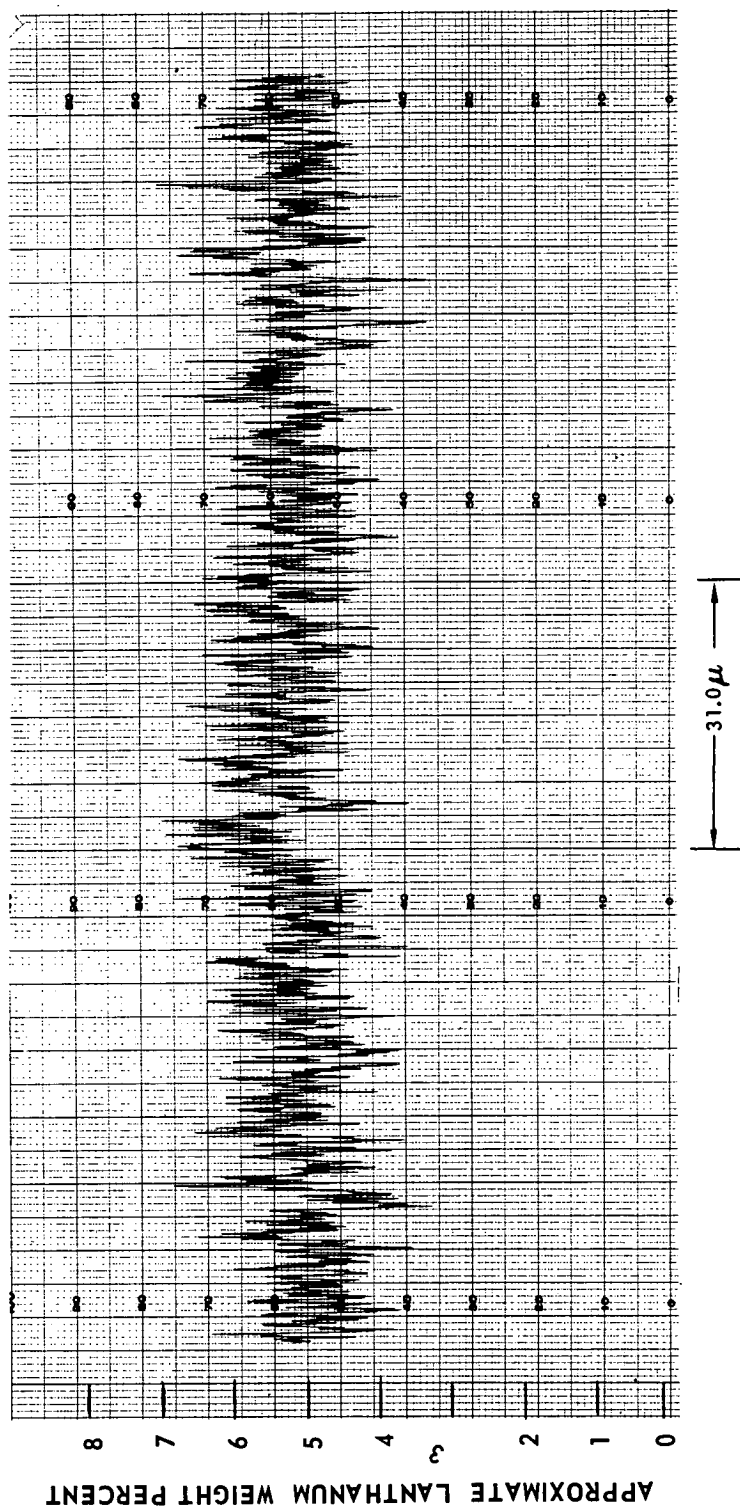


LANTHANUM DISTRIBUTION SCANS ACROSS PATH SHOWN SCHEMATICALLY IN FIG. 19



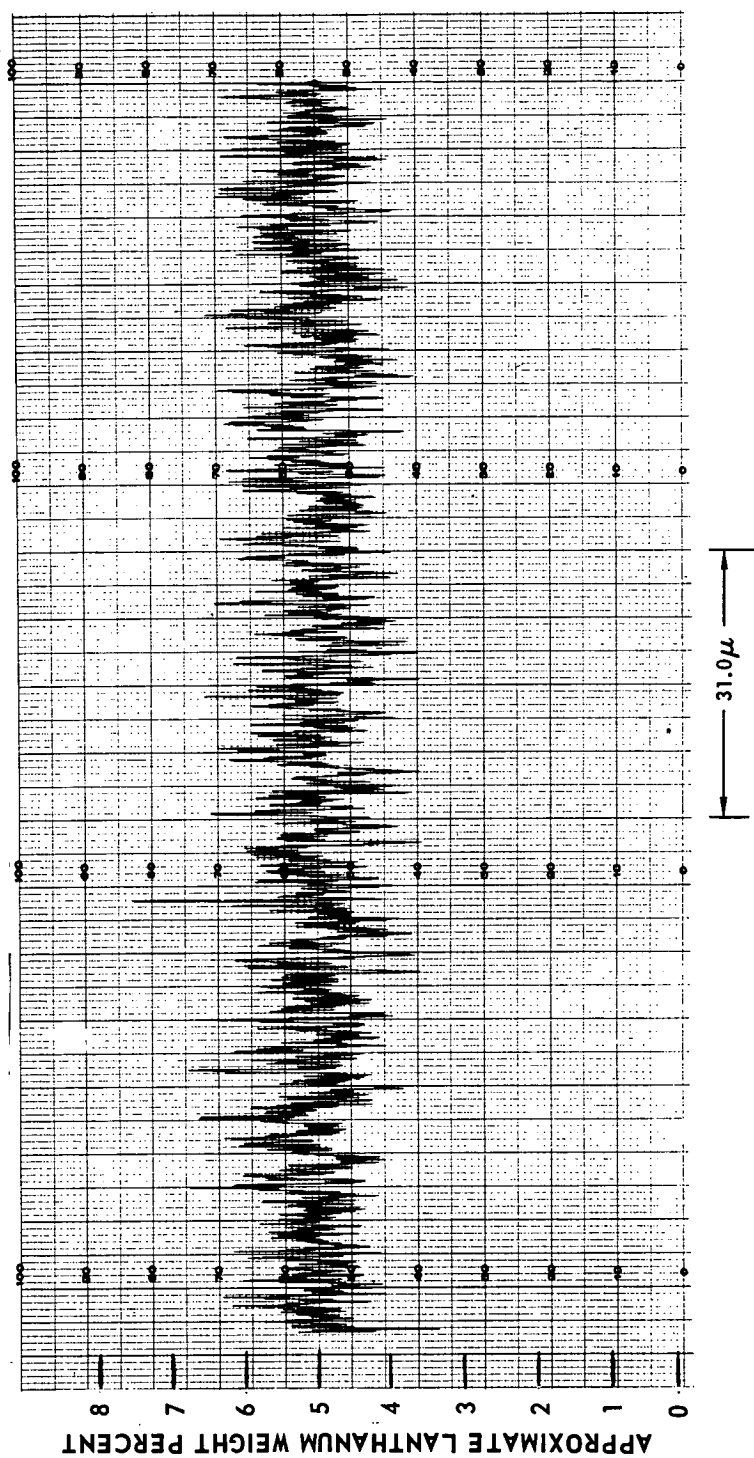
LANTHANUM DISTRIBUTION SCANS ACROSS PATH SHOWN SCHEMATICALLY IN FIG. 19

SCAN 5



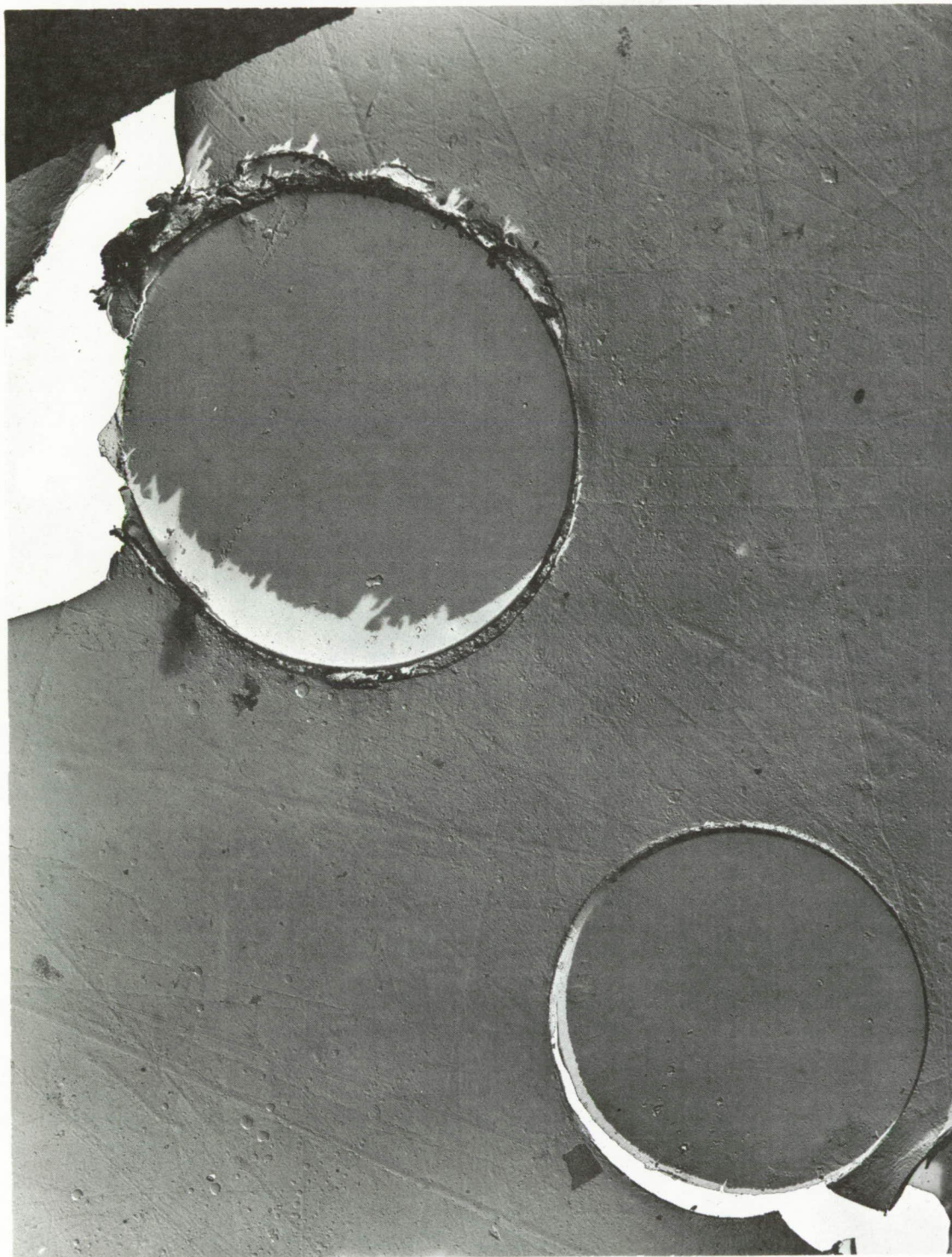
LANTHANUM DISTRIBUTION SCANS ACROSS PATH SHOWN SCHEMATICALLY IN FIG.19

SCAN 6



LANTHANUM DISTRIBUTION SCANS ACROSS PATH SHOWN SCHEMATICALLY IN FIG.19

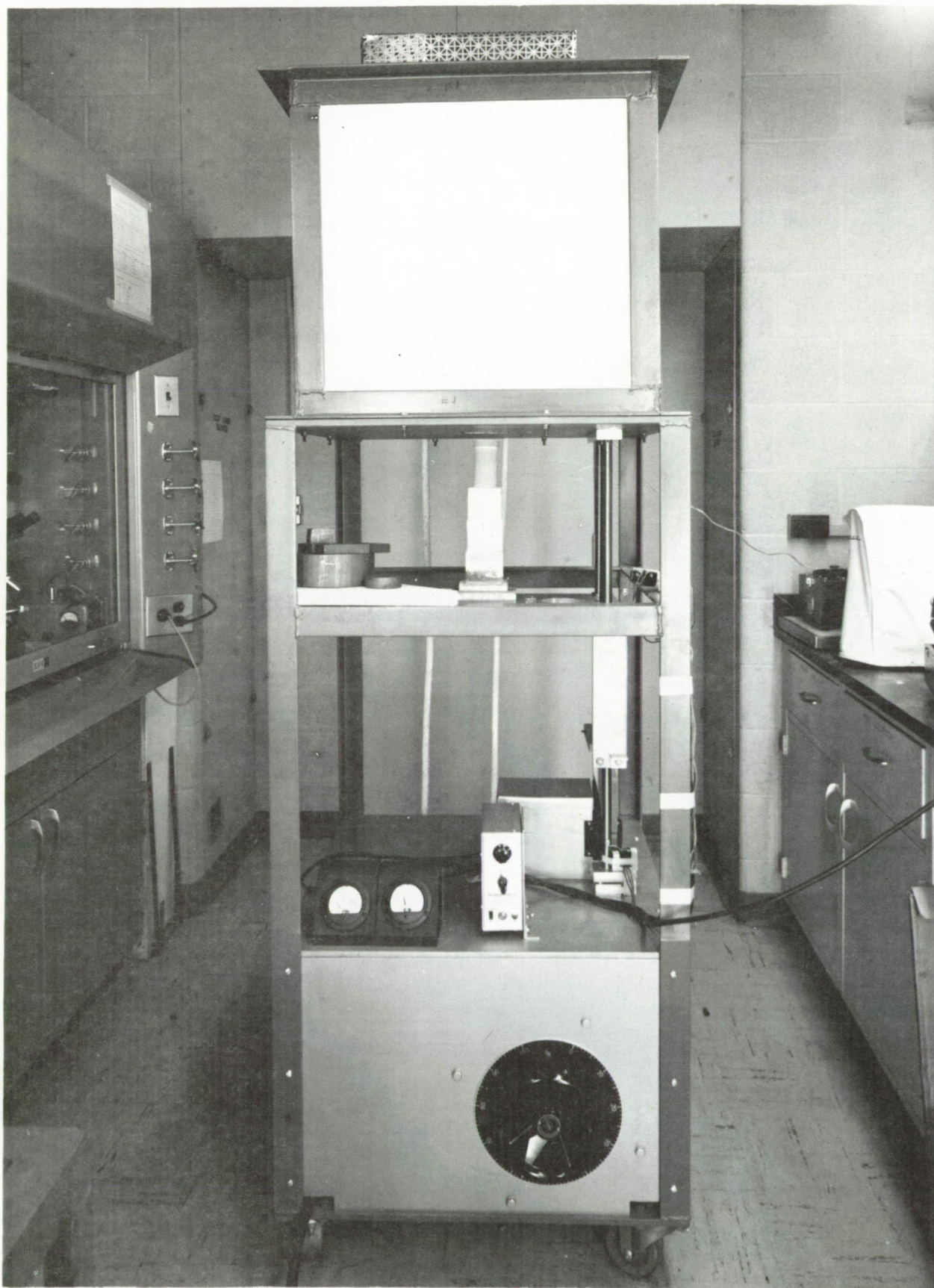
DEMONSTRATION OF CIRCULARITY OF MECHANICALLY DRAWN FIBERS



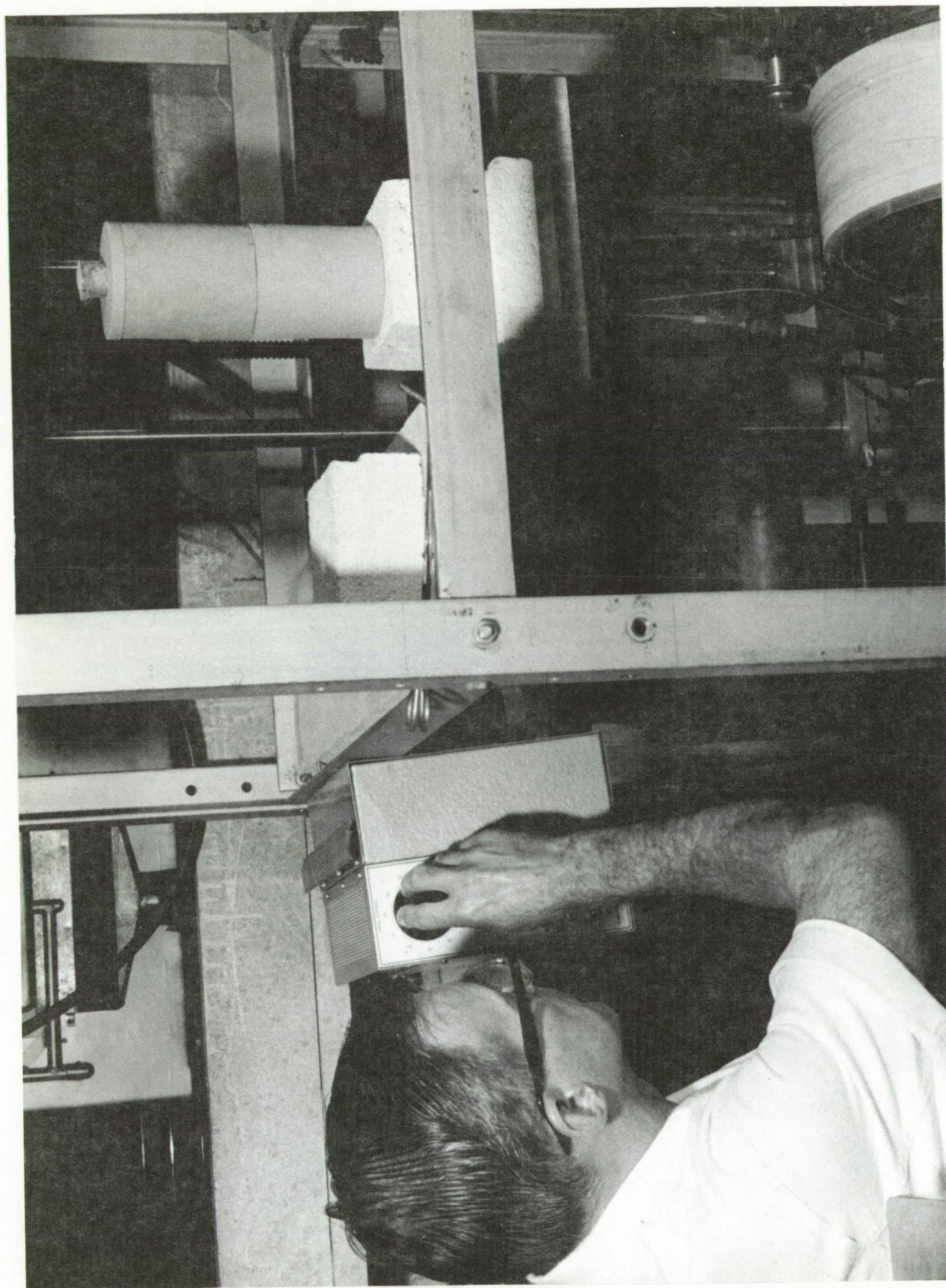
ELECTRON MICROGRAPH, 4500X

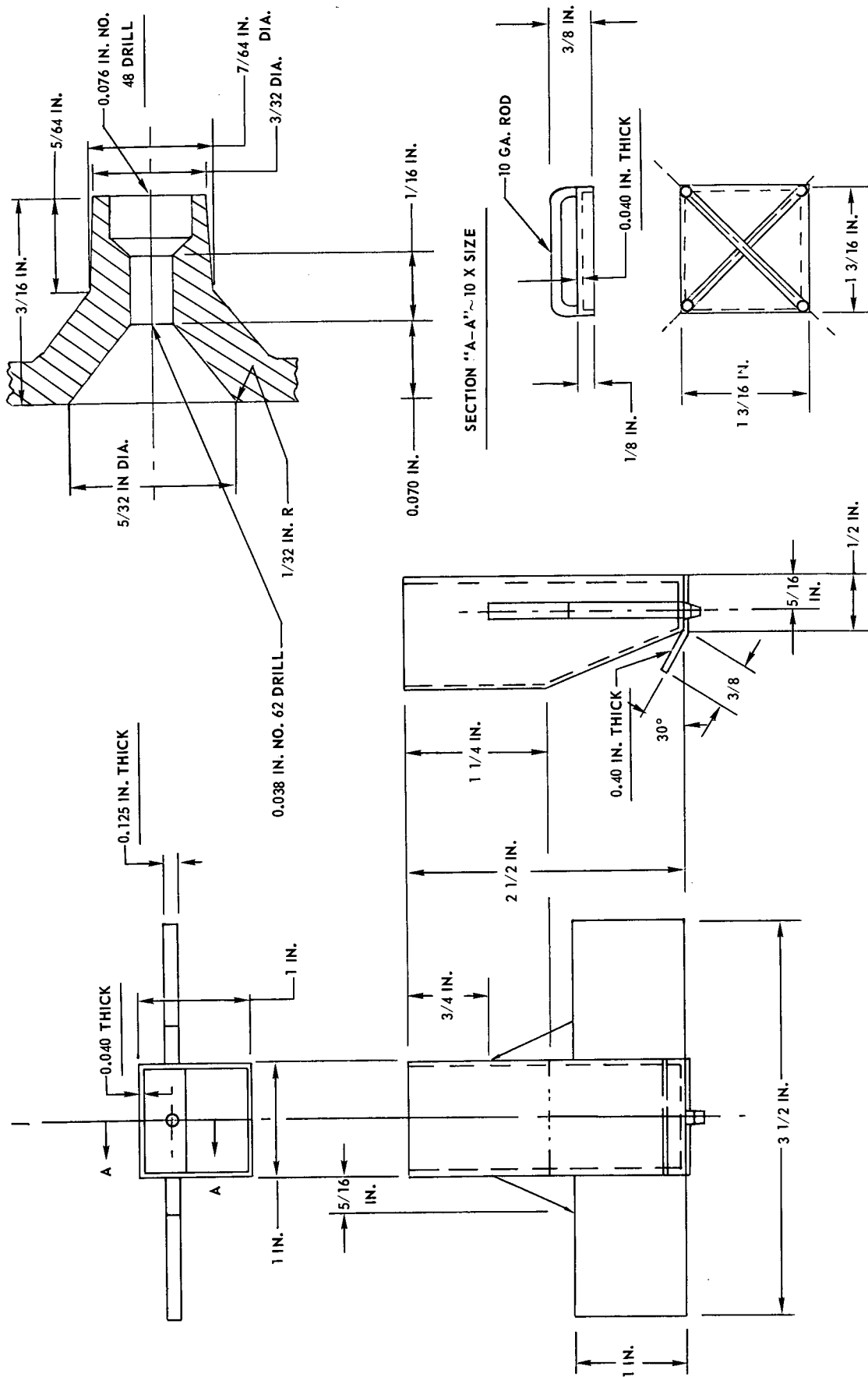
UARL 275-3 EXPERIMENTAL GLASS

PLATFORM KILN USED FOR FIBERIZABILITY STUDIES



PLATFORM KILN IN USE FOR MECHANICALLY DRAWING GLASS FIBERS





UARL DESIGN FOR SINGLE-HOLE BUSHING PATTERNED AFTER THOSE OF TIEDE (REF. 32) AND NAT. BUR. STANDARDS (REF. 33)